JGR Planets

RESEARCH ARTICLE
10.1029/2021JE007021

Key Points:

- Ancient fluvial systems on the dichotomy boundary in Memnonia Sulci, Mars, comprise valley networks, paleolake basins, and sediment fans
- The large fluvial catchment was subject to multiple periods of incision and aggradation, from the Noachian to Hesperian
- The downslope sediment fans are consistent with forming in paleolake basins, rather than a large regional sea or ocean

Supporting Information:

Supporting Information may be found in the online version of this article.

Correspondence to:

J. M. Davis,
joel.davis@nhm.ac.uk

Citation:

Davis, J. M., Aranos, L., Dickeson, Z. I., & Fawdon, P. (2022). The evolution of ancient fluvial systems in Memnonia Sulci, Mars: Impact crater damming, aggradation, and a large water body on the dichotomy? *Journal of Geophysical Research: Planets*, *127*, e2021JE007021. https://doi.org/10.1029/2021JE007021

Received 4 AUG 2021
Accepted 16 JAN 2022

Author Contributions:

Conceptualization: Joel M. Davis
Formal analysis: Joel M. Davis
Investigation: Joel M. Davis, Liliana Aranos
Methodology: Joel M. Davis, Liliana Aranos, Zachary I. Dickeson
Supervision: Joel M. Davis
Writing – original draft: Joel M. Davis
Writing – review & editing: Zachary I. Dickeson, Peter Fawdon

The Evolution of Ancient Fluvial Systems in Memnonia Sulci, Mars: Impact Crater Damming, Aggradation, and a Large Water Body on the Dichotomy?

Joel M. Davis[1], Liliana Aranos[2], Zachary I. Dickeson[1,3], and Peter Fawdon[4]

[1]Department of Earth Sciences, Natural History Museum, London, UK, [2]Department of Earth Science and Engineering, Imperial College London, London, UK, [3]Department of Earth and Planetary Sciences, Birkbeck, University of London, London, UK, [4]School of Physical Sciences, The Open University, Milton Keynes, UK

Abstract There is conflicting evidence for an ancient ocean which occupied the northern hemispheric basin on Mars. Along different regions of the dichotomy boundary, sediment fans have been interpreted as either forming into a large water body or a series of smaller paleolake basins. Here, we investigate fluvial systems in the Memnonia Sulci region of Mars, set along the dichotomy, which comprise erosional valley networks, paleolake basins, inverted channel systems, and sediment fans. We focus our analysis on the evolution of the upslope catchment and characterizing the ancient environment of a large, downslope basin, bound by the topographic dichotomy and the Medusae Fosse Formation. The catchment fluvial systems comprise highly degraded valley networks and show a complex history of incision and filling, influenced by paleolake basin overflow, impact crater damming, aggradation, and possibly a downstream water body. The morphology of the sediment fans is consistent with either fluvial fans or deltas and they form at discrete elevations, rather than a common elevation plane. Our analysis is consistent with the sediment fans forming into a series of paleolake basins set along the dichotomy, rather than into a large inner sea or ocean-sized water body. The fluvial systems were likely active between the mid Noachian and early Hesperian periods. Our results demonstrate the complex, multi-phase evolution of fluvial systems on ancient Mars and highlight the importance of regional and local studies when characterizing ancient regions of the dichotomy.

Plain Language Summary The northern third of Mars contains an extensive topographic basin, but there is conflicting evidence to whether it was once occupied by an ocean-sized body of water billions of years ago. At the margins of this basin are the remnants of deltas, which formed into water, but the size and nature of this water body (or water bodies) is unclear, and detailed investigations of different regions of the basin margins are necessary. In this study, we use high-resolution image and topographic datasets from satellites orbiting Mars to investigate a series of water-formed landforms in the Memnonia Sulci region, set along the boundary of Mars's northern basin. These landforms likely formed billions of years ago, providing evidence for ancient rivers and lakes in this region. The geologic evolution of these rivers and lakes was complicated, likely influenced by water-level fluctuations, changes in sediment availability, and impact cratering. Our topographic analysis of these rivers and lakes suggests that they terminated in a series of ancient lake basins at the boundary of Mars's northern basin, rather than supplying a larger, ocean-sized body of water. Our results highlight the importance of regional and local studies when characterizing the margins of Mars's northern basin.

1. Introduction

The geologic record of Mars points to an early history strongly influenced by aqueous processes. This record includes degraded impacts craters, consistent with fluvial erosion (Craddock et al., 1997; Howard et al., 2005), erosional valley networks (Craddock & Howard, 2002; Hynek et al., 2010; Irwin & Howard, 2002), depositional channel systems (Balme et al., 2020; Burr et al., 2010; Williams et al., 2009), paleolake basins (Fassett & Head, 2008; Goudge et al., 2016; Grotzinger et al., 2015; Stucky de Quay et al., 2020), sediment fans (Davis et al., 2021; Goudge et al., 2016; Rice et al., 2013; Wilson et al., 2021), and hydrated mineral deposits (Bibring et al., 2006; Ehlmann & Edwards, 2014). However, there is conflicting evidence for an ancient ocean filling the northern hemispheric basin of Mars (Carr & Head, 2003; Clifford & Parker, 2001; Parker et al., 1993; Sholes et al., 2021). One of the most intriguing lines of evidence for such a water body are sediment fans—candidate deltas—along the martian dichotomy, the margins of any potential ocean. Di Achille and Hynek (2010) identified

52 candidate deltas along the dichotomy at a similar elevation plane, consistent with a former shoreline for a large, standing body of water in the northern lowlands. This interpretation is complicated by subsequent, global-scale tectonic deformation (Citron et al., 2018). Recent regional and local studies have built on the work of Di Achille and Hynek (2010) by providing detailed geologic, physiographic, and temporal characterization of these candidate deltas.

In Xanthe Terra, the sediment fan at the terminus of Hypanis Vallis, a late Noachian to early Hesperian age valley network, was characterized as an exhumed deltaic deposit (Adler et al., 2019; Fawdon et al., 2018). The Hypanis delta may have formed into a large, receding body of water which spanned the northern lowlands (Fawdon et al., 2018). In Aeolis Dorsa, depositional channels and deltas also support the presence of a large, downstream water body (Cardenas et al., 2017; DiBiase et al., 2013; Hughes et al., 2019). To contrast, Rivera-Hernández and Palucis (2019) and García-Arnay and Gutiérrez (2020) found that numerous deltas in the Gale crater region occur at multiple, discrete elevations, suggesting they formed into several paleolake basins, rather than a regional sea or large ocean. These differing interpretations highlight the importance of detailed, regional studies which characterize fluvial systems along the dichotomy (Dickeson & Davis, 2020).

Here, we investigate a series of fluvial systems along the dichotomy boundary in the Memnonia Sulci region of Mars using high-resolution image and topographic datasets. The fluvial systems in this region have previously been investigated (Irwin et al., 2005; Ori et al., 2000), however, these studies were prior to the widespread coverage of high-resolution datasets, which could give new insight into their evolution. The fluvial systems comprise valley networks, paleolake basins, inverted channel systems, and sediment fans, which debouch into a large basin bound by the Medusae Fosse Formation (MFF) to the north and the dichotomy to the south (Figure 1). We investigate the upslope catchment and the influences on its evolution, and the relationship to regional stratigraphic units and use impact crater size-frequency distributions to constrain the age of the fluvial systems. Finally, we use the sediment fans to characterize the nature of the MFF-dichotomy bound basin and consider the implications for a northern ocean on early Mars.

2. Regional Geology of Northwest Memnonia Sulci

Our study region is situated in the northwest section of the Memnonia quadrangle (Figure 1). Here, the highland terrain south of the dichotomy is mid-Noachian in age (3.9–3.8 Ga; Tanaka et al., 2014) and contains numerous, large, degraded impact craters. Erosional valley networks in the region converge on and debouch at the dichotomy (Alemanno et al., 2018; Hynek et al., 2010). Previous authors have identified multiple open paleolake basins situated within the erosional valley networks here (Irwin et al., 2005; Ori et al., 2000).

North of the dichotomy are exposures of the Medusae Fosse Formation (MFF), a regionally extensive, extremely friable unit. The formation mechanism for the MFF is unknown and potential emplacement mechanisms include as pyroclastic flows, ashfall or ash flow (e.g., Kerber & Head, 2010; Ojha & Lewis, 2018) or aeolian deposits (e.g., Scott & Tanaka, 1986). Within the MFF, there is extensive evidence for (1) widespread aeolian re-working (e.g., Mandt et al., 2008; Zimbelman & Griffin, 2010) and, in Aeolis Dorsa, at the western margin of the MFF, re-working by fluvial processes (e.g., Kerber & Head, 2010; Lefort et al., 2012).

Northwest Memnonia is adjacent to Lucus Planum, a central exposure of the MFF (Figure 1b). Stratigraphic relationships indicate that the Lucus Planum section of the MFF was likely emplaced and modified from the Hesperian (3.7–3.0 Ga) to Amazonian (3.0–0 Ga) periods (Kerber & Head, 2010; Tanaka et al., 2014). Lucus Planum and the hemispheric dichotomy together form an WSW-ENE orientated basin, which runs for 500 km along its longest axis (Figure 1b). Although much of this basin is topographically enclosed, at its NE margin it intersects the northern lowlands. Our main study area is situated at the SW margin of this basin.

3. Data and Methods

3.1. Datasets

We investigate the fluvial systems in the Memnonia Sulci region primarily using Context Camera (CTX; 5–6 m/pixel; Malin et al., 2007) and High Resolution Imaging Science Experiment (HiRISE; 0.25 m/pixel; McEwen et al., 2007) datasets. We combined eight CTX images to produce a mosaic basemap for the main

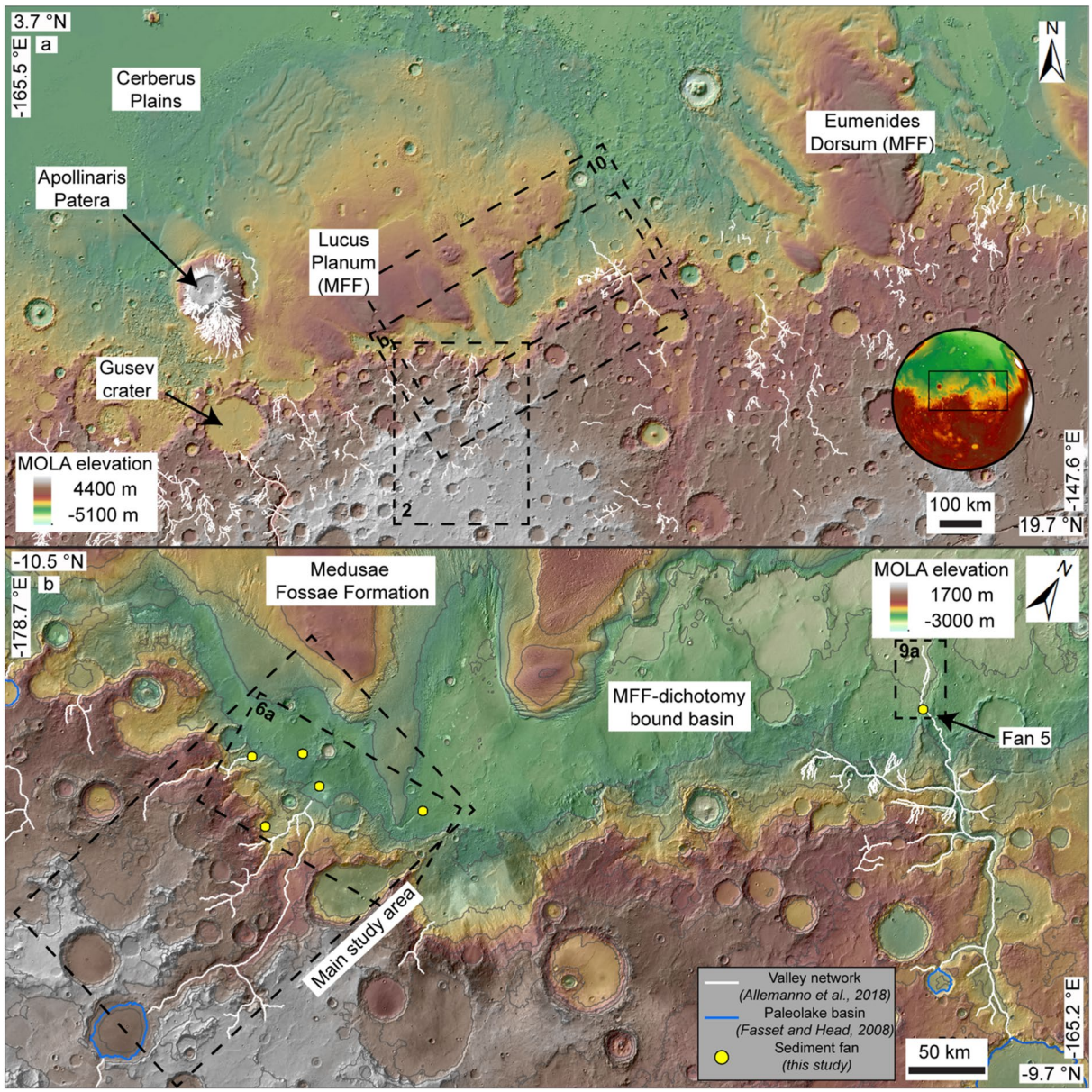

Figure 1. (a) MOLA topography overlaid on shaded relief showing Memnonia region of Mars. The ancient, cratered highlands are visible in the south. North of the dichotomy is the Medusae Fosse Formation (MFF). (b) MOLA topography overlaid on THEMIS-IR day mosaic of NW Memnonia region. A WSW-ENE trending basin is visible bounded between the MFF to the north and the dichotomy boundary to the south. The main study region is shown by the black dashed line. Contours shown at 500 m intervals.

study area. We produced HiRISE and CTX digital elevation models (DEMs; Table S1 in the Supporting Information S1) of the fluvial catchment and sediment fans using the USGS Integrated Software for Imagers and Spectrometers (ISIS) software and the BAE photogrammetric package SOCET SET (Kirk et al., 2008). The resultant DEMs were tied to Mars Orbital Laser Altimeter (Zuber et al., 1992) topography and exported with a post spacing of 1 and 20 m/pixel for HiRISE and CTX, respectively. These DEMs were supplemented by MOLA topography (450 m/pixel). We used CTX and MOLA topography to measure the along and cross-section profiles of the catchment fluvial systems. We also used available Color and Stereo Science Imaging System (CaSSIS; 4.5 m/pixel; Thomas et al., 2017) images to investigate the sediment fans. We used images with the combined NIR-BLU-PAN filters (NBP) and synthetic RGB images created from the BLU and PAN filters. Our investigation

was also supplemented by the global THermal Emission Imaging System (THEMIS; 100 m/pixel; Christensen et al., 2004) mosaic.

3.2. Measurements of the Fluvial Catchment

Within our main study area (Figure 1), we used the valley networks mapped by Alemanno et al. (2018) to identify the largest and most continuous of the catchment fluvial systems, which we refer to as Unnamed Valley 1 (UV1). We used the standard ArcGIS hydrology toolkit to measure the possible drainage catchment of UV1 using the MOLA DEM clipped to the western Memnonia region. We filled the DEM to a depth of 750 m to account for local hydrological sinks (value determined based on deepest sink; B1) and to ensure continuous flow. Our fill value was defined based on the maximum depth of a 50 km diameter open basin paleolake, midway along the course of UV1. To define a watershed, we placed a pour point near the outlet of UV1. Finally, we compared our watershed to the morphological expression of valley networks. As the ArcGIS hydrology toolkit is designed for active river systems on Earth and not ancient topography on Mars, we consider our hydrology measurements as a rough guide to the potential size of the catchment.

3.3. Age Estimates From Geologic Maps and Impact Crater Size-Frequency Distributions

Estimating when small or linear features such as valley networks or sediment fans formed using impact crater size-frequency distributions ("crater counting") is challenging and can produce misleading results (e.g., Warner et al., 2015). Instead, we mostly rely on the stratigraphy of published geological maps (Tanaka et al., 2014) to estimate when fluvial processes were occurring. We do perform one crater count of an 18 km diameter impact crater (Crater A) which overlies the fluvial catchment and has well-defined impact ejecta. We mapped out the impact ejecta, before counting all overlying craters visible in our CTX mosaic using the ArcMap extension CraterTools (Kneissl et al., 2011) which were greater than 50 m in diameter. We then used CraterStats2 (Michael et al., 2012) software to produce a model formation age for Crater A, using the production function of Ivanov (2001) and the chronology function of Hartmann and Neukum (2001).

4. Observations and Results

To constrain the ancient environment in this region of the dichotomy, we investigate the fluvial catchment (4.1), its minimum age (4.2), and the sediment fans fed by the catchment (4.3).

4.1. Catchment of the Fluvial Systems

In this section, we describe the catchment fluvial systems within the main study area, which fed the downslope sediment fans and the MFF-dichotomy bound basin. Erosional valley networks in this region converge on the dichotomy (Allemanno et al., 2018; Hynek et al., 2010, Figure 1). The longest of the systems within our main study area, Unnamed Valley 1 (UV1), was fed by a watershed potentially 58,000 km^2 in area and extended 450 km south of the dichotomy (Figures 2 and 3). In the lower reaches of UV1, our reconstructed catchment area mostly coincides with the morphological expression of valley networks (Figure 2). To contrast, valley networks are largely absent from the upper reaches of the reconstructed catchment, although there are some examples of degraded basins with outlet valleys (Figure 2). Approximately midway along the course of UV1 is a degraded, flat-floored 50 km impact crater, with multiple sets of terraced structures around its interior rim (Figure 2). This crater is breached by UV1 at both its northern and southern margins and has previously been interpreted as an open paleolake basin (Irwin et al., 2005; Ori et al., 2000). We refer to this open paleolake basin as Basin 1 (B1). The morphology of UV1 is consistent with an erosional valley network formed by fluvial erosion (e.g., Allemanno et al., 2018; Hynek et al., 2010).

We focus our observations on the 190 km long section of UV1 north of B1, which continues toward the dichotomy (Figure 3). The walls of UV1 here are poorly defined but appear controlled by ancient crater rims and ejecta blankets (Figure 2). Paired erosional terrace structures which run parallel to the valley walls are sometimes present in some of this northern section (Figures 3b and S1 in the Supporting Information S1). The valley floor of

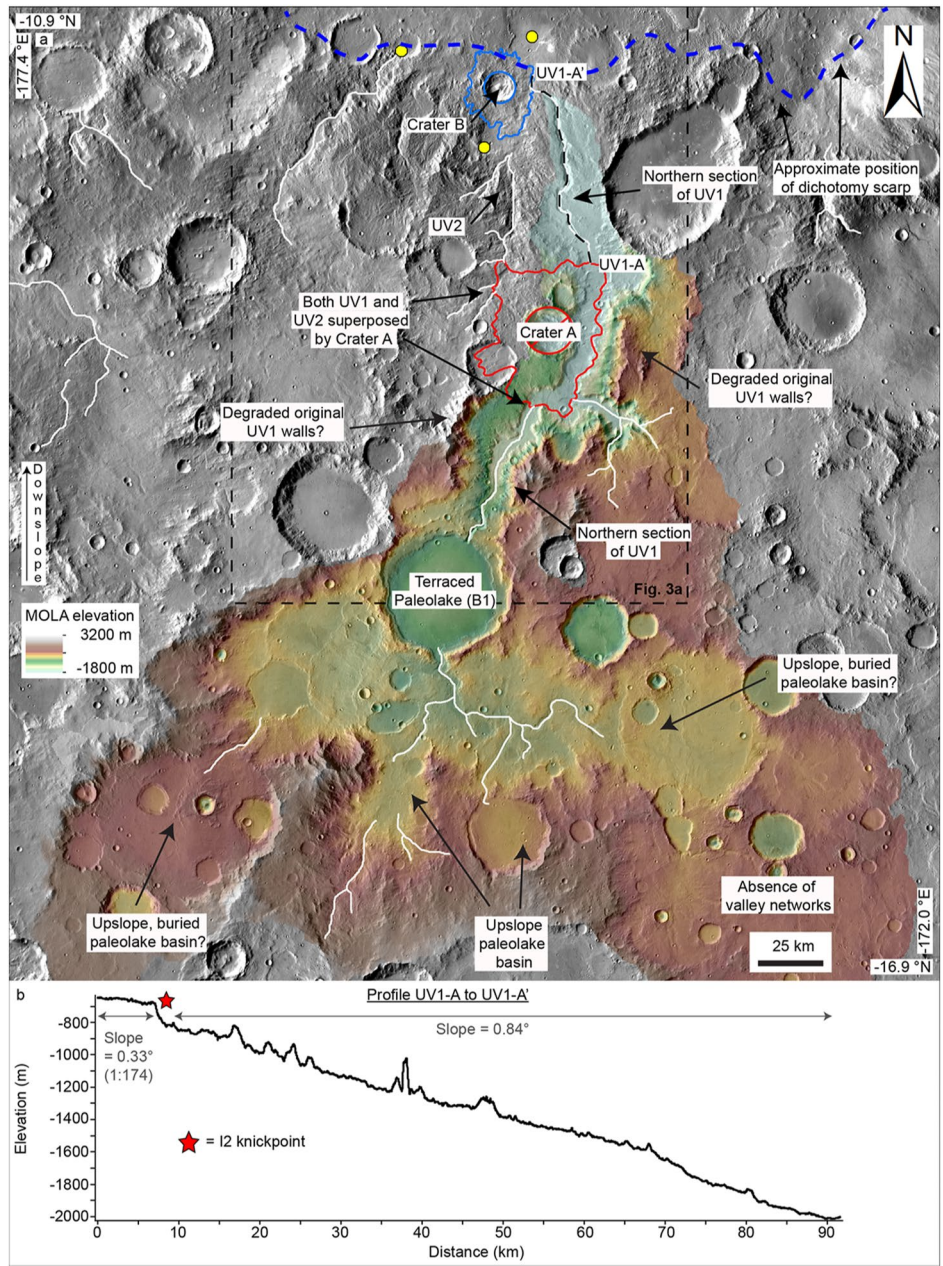

Figure 2. (a) MOLA topographic map clipped to the modeled hydrological catchment of Unnamed Valley 1 (UV1) overlaid on a THEMIS-IR day basemap. The catchment of U1 is 58,000 km^2 in size and in its lower reaches coincides with the morphological expression of UV1 (white lines; modified from Alemanno et al. (2018)). UV1 likely supplied the downslope sediment fans (yellow circles). Valley network adjacent to UV1 have significantly less reach and impact cratering has obscured much of their pathways. (b) Topographic profile (UV1-A to UV1-A'; dashed black line) along section of UV1. The gradient of UV1 increase nearly threefold at the knickpoint where I2 begins (red star). Profile extracted from a CTX DEM.

UV1 appears infilled (Figure 3), although in two locations, this valley infill is incised. The first of these incised sections begins at the paleolake outlet (I1) and continues for approximately 60 km (Figure 3b). The incision depth of I1 shallows as it increases with distance from B1 (from ~300 m depth at B1 to 0; Figure 3). I1 eventually intersects an 18 km diameter impact crater (Crater A) which superposes both UV1 and I1 (Figure 3). The ejecta from Crater A appears mostly unmodified and does not appear to have been subsequently incised.

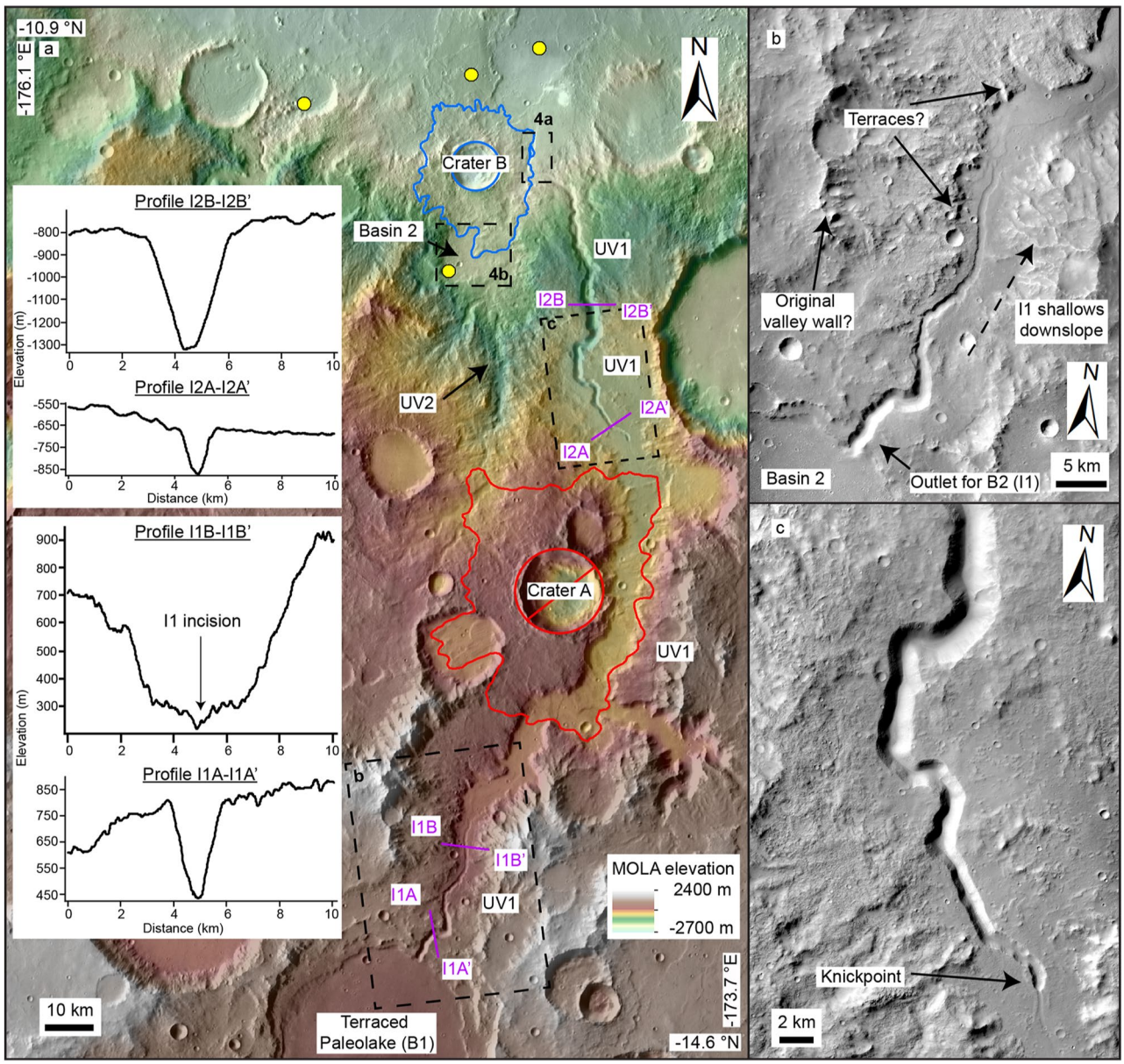

Figure 3. Unnamed Valley 1. (a) MOLA topography overlaid on THEMIS-IR day mosaic showing the northern section of UV1, which begins at Basin 1 (B1). Crater A (red outline) superposes UV1 and has not been incised. Crater B (blue lines) also superposes UV1 but has subsequently been incised. Cross-sectional profiles show sections where the fill of UV1 has been incised (I1 and I2). Profiles were extracted from two CTX DEMs. Yellow circles show sediment fan locations. (b) CTX mosaic of I1 which begins at the outlet for the terraced paleolake (B 1), shallowing in the downslope direction (Profiles I1A-I1A′ and I1B-I1B′). The original walls are highly degraded, and terrace structures are visible. (c) CTX image showing the southern section of I2, which begins at a knickpoint north of Crater A. I2 initially deepens (Profiles I2A-I2A′ and I2B-I2B′) before shallowing.

The second incised section (I2) of UV1 begins at a knickpoint approximately 70 km south of the valley mouth (north of Crater A), where there is a significant increase in gradient (Figure 2b). I2 initially deepens to a maximum depth of 600 m before shallowing (Figure 3a). At its northern end, I2 is superposed by ejecta from a 12 km diameter impact crater (Crater B; Figure 3a). However, the ejecta which superposes I2 is not continuous and appears to have been incised since its formation (Figure 4a). A 5 km long ridge is situated within I2, which also superposes the Crater B ejecta (Figure 4a). The ridge is 50–150 m wide and some discontinuous ridge segments are observed within I2 further upslope. Little to no structure is exposed in the top surface or margins of the ridges. As the ridges are situated within I2, we interpret them as inverted channel deposits (deposits of indurated fluvial

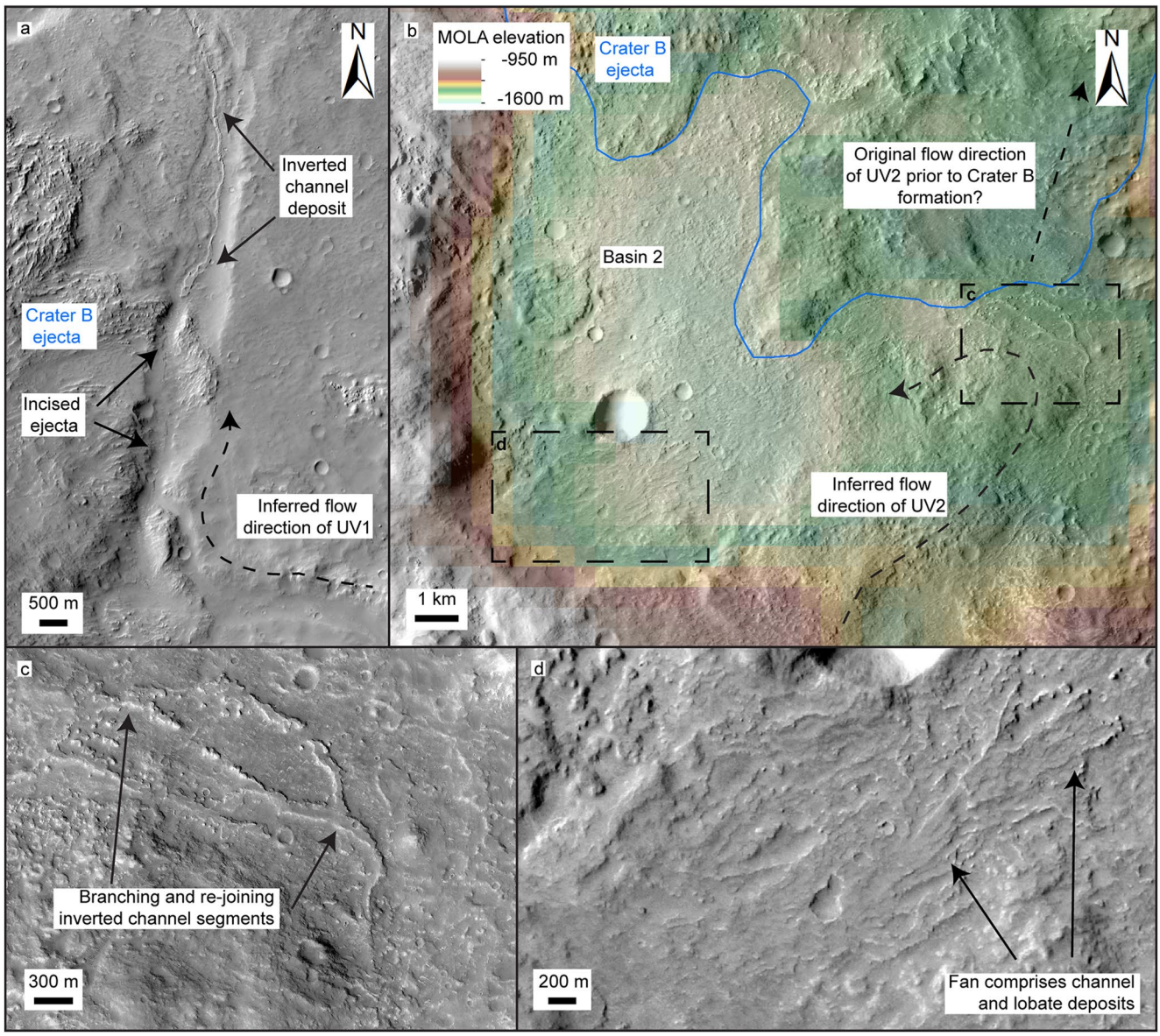

Figure 4. Lower reaches of UV1 and UV2. (a) CTX mosaic showing lower reaches of UV1 near the dichotomy. I2 shallows here and has been infilled by Crater B ejecta. However, the ejecta has subsequently been incised and a 5 km long inverted channel system fills this section of I2. (b) MOLA topography overlaid on CTX mosaic of Basin 2. UV2 abruptly changes direction to the SW and enters Basin 2 as it nears the ejecta from Crater B. (c) HiRISE image of branching and re-joining inverted channel segments, which infill UV2 near the eastern margin of Basin 2. (d) CTX image of sediment fan comprising channel and lobate deposits at the SE margin of Basin 2.

sediment exhumed by differential erosion) and their morphology is consistent with other examples of Mars (e.g., Burr et al., 2010; Davis et al., 2016; Hayden et al., 2019; Williams et al., 2009).

North of Crater B, I2 debouches onto a plain bound by the MFF and the dichotomy scarp. South of Crater B is an additional valley network, which we refer to as Unnamed Valley 2 (UV2). UV2 is approximately 80 km in length and runs approximately parallel to UV1 (Figures 2 and 3a). Like UV1, UV2 has also been heavily modified since its formation and attempts to reconstruct its watershed were unsuccessful. Near its uppermost reach, parts of UV2 have been completely buried by Crater A (Figure 2). As UV2 approaches Crater B, its abruptly changes direction to the SW, where it debouches into a 13 km diameter basin, Basin 2 (B2; Figure 4b). B2 appears to be a highly degraded impact structure. At the eastern margins of B2 are branching and re-joining ridge segments, approximately 10 km long, situated within the fill of UV2 (Figure 4c). As with the previous example in UV1, we

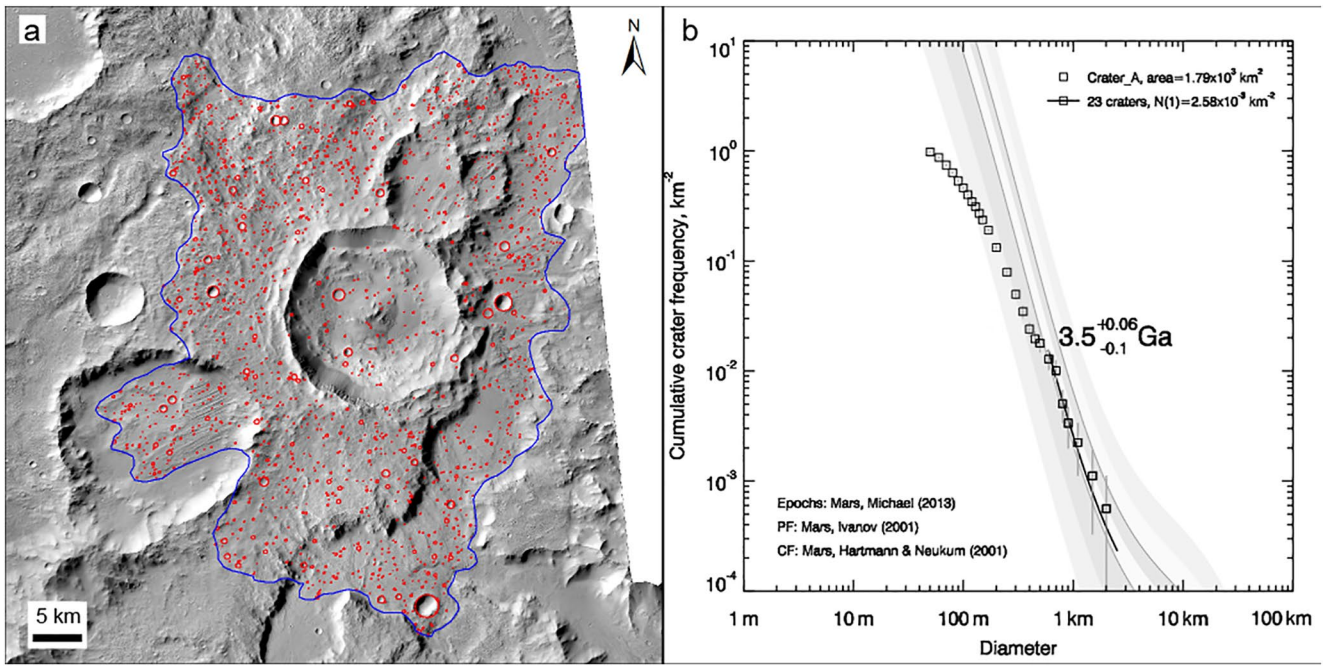

Figure 5. Crater count of Crater A. (a) Mosaic of CTX images showing extent of the ejecta from Crater A which superposes Unnamed Valley 1 (blue line). The red circles show all craters ($D \geq 50$ m) measured in CraterTools which superpose Crater A. (b) Binned cumulative crater frequency histograms for Crater A. Modeled ages are based on the isochrons defined by Hartmann and Neukum (2001) and using the chronology of Michael (2013). 23 of the largest craters show a best fit to the 3.5 ± 0.1 Ga isochron.

interpret these ridges as inverted channel deposits. At the SW edge of B2, there is a 5 km long, poorly exposed, fan-like form, comprised of channel and lobate structures (Figure 4c).

4.2. Minimum Age of the Fluvial Catchment

In this section, we use crater counting to constrain the minimum age of the catchment. Crater A superposes and infills UV1 and UV2, and its impact ejecta does not appear incised. Crater A and its ejecta cover an area of 1.79×10^3 km^2. Figure 5 shows the count area and the binned cumulative crater frequency histograms for Crater A. In total, we counted 1,755 craters ($D \geq 50$ m) which were overlying Crater A. Of these, the largest craters ($n = 23$) fall along the 3.5 ± 0.1 Ga isochron, defined by Hartmann and Neukum (2001) and using the chronology of Michael (2013).

4.3. Description and Interpretation of the Sediment Fans

In this section, we describe and interpret the major sediment fans found along the dichotomy in this region. Figure 6a shows the locations of fans in the main study area.

4.3.1. Fan 1

Observations: Fan 1 begins 10 km north of UV1 outlet (Figure 6a). Fan 1 comprises a series of linear to quasi-sinuous ridges, orientated in the downslope direction (Figure 6b). The ridges are approximately 50–200 m wide, ~5 m high, and form 2–5 km long continuous segments. The ridges progressively bifurcate in the downslope direction (Figure 6c) and multiple ridge systems superpose one another (Figure 6b). Approximately a third of the way downslope, Fan 1 divides into two main branches, Branch A and B (Figure 6b). Branch A appears stratigraphically higher than Branch B. The distal section of Branch B is ~20 m lower in elevation than Branch A. There are also examples of ridges amalgamated together laterally (Figure 6c). At the downslope termination of Branch A, some ridges bifurcate into narrower, digitate ridges (Figure 6d). In the distal region of Branch B, the

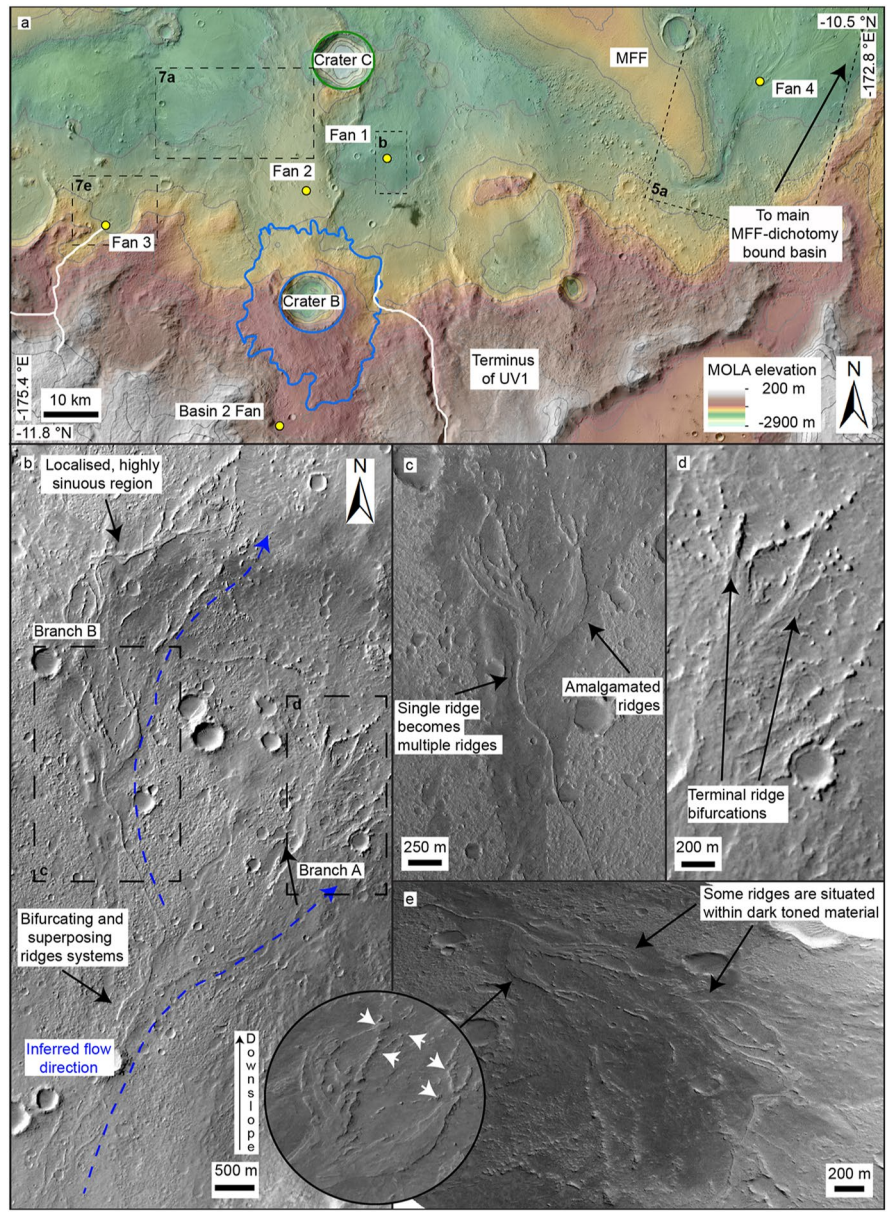

Figure 6. Context location of sediment fans and Fan 1. (a) MOLA topography overlaid on CTX mosaic showing locations of sediment fans (yellow circles) found at the margins of the MFF-dichotomy bound basin and near the terminus of Unnamed. (b) CTX mosaic of Fan 1, which is 16 km long. Ridge structures bifurcate in the downslope direction. The dashed blue line shows the inferred flow direction. Branch B is stratigraphically higher than Branch A. (c) HiRISE image showing section of Fan 1, where a single ridge transitions into multiple ridge structures. Some of these ridges form laterally amalgamated systems. (d) CTX image showing eastern terminus of Fan 1, where the ridges bifurcate into narrow, shorter ridges. (e) Oblique view of northern section of Fan 1 facing upslope. The image was constructed from HiRISE topography pansharpened with a synthetic RGB CaSSIS image. Inset shows oblique HiRISE topography where ridge stacking is apparent.

ridges show a higher degree of sinuosity (Figure 6b). Adjacent and parallel to some of the ridges are corridors of darker material (Figures 6c and 6d). The ridges are set within low relief plains and appear to being exhumed from a mid-toned material, with a distinct mottled and pitted surface texture (Figure 6b). At its longest extent, Fan 1 extends 16 km from its southern to northern most point, over an average slope of 0.3° (1:190).

Interpretation: Due to their sinuous and branching nature and their proximity to the upslope fluvial systems, we interpret the ridges as inverted channel systems (e.g., Burr et al., 2010; Davis et al., 2016; Williams et al., 2009).

We further interpret the ridges as the exhumed remnants of a distributary channel and sediment fan system. The occurrence of Fan 1, 10 km north of the UV1 outlet, set within low relief plains, could be consistent with either an aggrading fluvial fan (e.g., Ventra & Clarke, 2018) or a delta (Fawdon et al., 2018). In this work, we consider a fluvial fan to comprise multiple, extensive, distributary fluvial systems (i.e., migrating and aggrading channel-belts) with low gradient surfaces and often fed by an extensive catchment (e.g., Ventra & Clarke, 2018). A delta is broadly similar to a fluvial fan, with the addition of forming into a standing body of water, resulting in some sediment stored below base level (e.g., Ganti et al., 2014; Ventra & Clarke, 2018). To contrast, alluvial fans often form adjacent to short, steep catchments and can have high, proximal surface gradients (Blair & McPherson, 1994).

4.3.2. Fan 2

Observations: Fan 2 begins at the end of a 25 km long NW trending channel, which originates from the outlet of UV1 (Figure 7a). The feeder channel appears to have been deflected around Crater C (Figure 7a), which likely pre-dates Fan 2. The main body of Fan 2 comprises a plethora of curvilinear, discontinuous ridges which significantly vary in orientation, although commonly WNW-ESW or NNW-SSE (Figures 7b and 7c). Ridges are up to 5 km long, ~50–300 m wide, and 5–10 m high (Figures 7b and 7c). The ridges occur on an expansive, planar surface, from which some ridges are being exhumed (Figure 7a). As in Fan 1, ridge systems divide in the downslope direction and commonly superpose one another (Figures 7c and 7d). In some examples, distinct caprock is visible on the ridges (Figure 7c). Multiple ridge systems appear to have amalgamated together laterally (Figures 7c and 7d). In total, the ridges cover an area of 18 km by 12 km, over an average slope of 0.005° ($1{:}1.1 \times 10^4$).

Interpretation: Of all the sediment fans in the study, we are least confident in our interpretation of Fan 2. The gradational boundary between the impact ejecta from Crater C and the ridges suggests that the ridges maybe eroded, distal ejecta deposits (e.g., Barlow et al., 2000). However, the orientation and planimetric pattern of some of the ridges are inconsistent with impact ejecta originating from Crater C. The curvilinear and bifurcating nature of some ridges, as well as the examples of multiple ridges amalgamated together are instead more consistent with the exhumed remnants of a distributary channel and sediment fan system (i.e., a fluvial fan). It is possible that Fan 2 may represent a sediment fan overlying ejecta deposits in places. Unlike Fan 1, Fan 2 forms northwest of UV1, away from the main MFF-dichotomy bound basin to the northeast (Figure 6a).

4.3.3. Fan 3

Observations: Fan 3 is found at the southwest interior margin of a highly degraded, 10 km impact crater approximately overlying the dichotomy, where an erosional valley network debouches (Figure 7e). The catchment for Fan 3 extends at least 20 km southwest. Fan 3 forms an arcuate shaped deposit, 3 km long by 6 km, filling the width of the crater (Figure 7e). Distal erosional remnants suggest that Fan 3 was previously more extensive and may have filled the diameter of the crater entirely. Erosion has exposed 50–100 m wide, curvilinear ridges which are generally orientated NNE (Figure 7f). At the margins of these ridges, sub-horizontal layering is exposed (Figure 7f). The northern wall of the crater has been eroded away and some of the ridges extended beyond the proximal fan deposits and outside the confines of the crater (Figure 7e).

Interpretation: The curvilinear ridges exposed in Fan 3 are consistent with inverted channel deposits. The morphology of Fan 3 is consistent with a fluvial fan or a delta body. As the distal deposits of Fan 3 steps out of the hosting crater, if it formed into a water body, such a body may not have been confined to the crater.

4.3.4. Fan 4

Observations: Fan 4 is found 70 km ENE of Fan 1 (Figure 6). The apex of Fan 4 is found ~100 m lower in elevation than the most distal sections of Fan 1 and at the end of a 35 km long feeder channel, the pathway of which suggests it has been diverted around at least some of the MFF (Figure 8a). The origin of the feeder channel is unclear as it appears buried at its upslope margin. Fan 4 comprises multiple, discrete, flat-topped sediment bodies, typically ~100–1,500 m wide and ~1–5 km long, orientated in the downslope direction (Figure 8b). Sub-horizontal layering is exposed in the margins of the sediment bodies, which is continuous for hundreds of

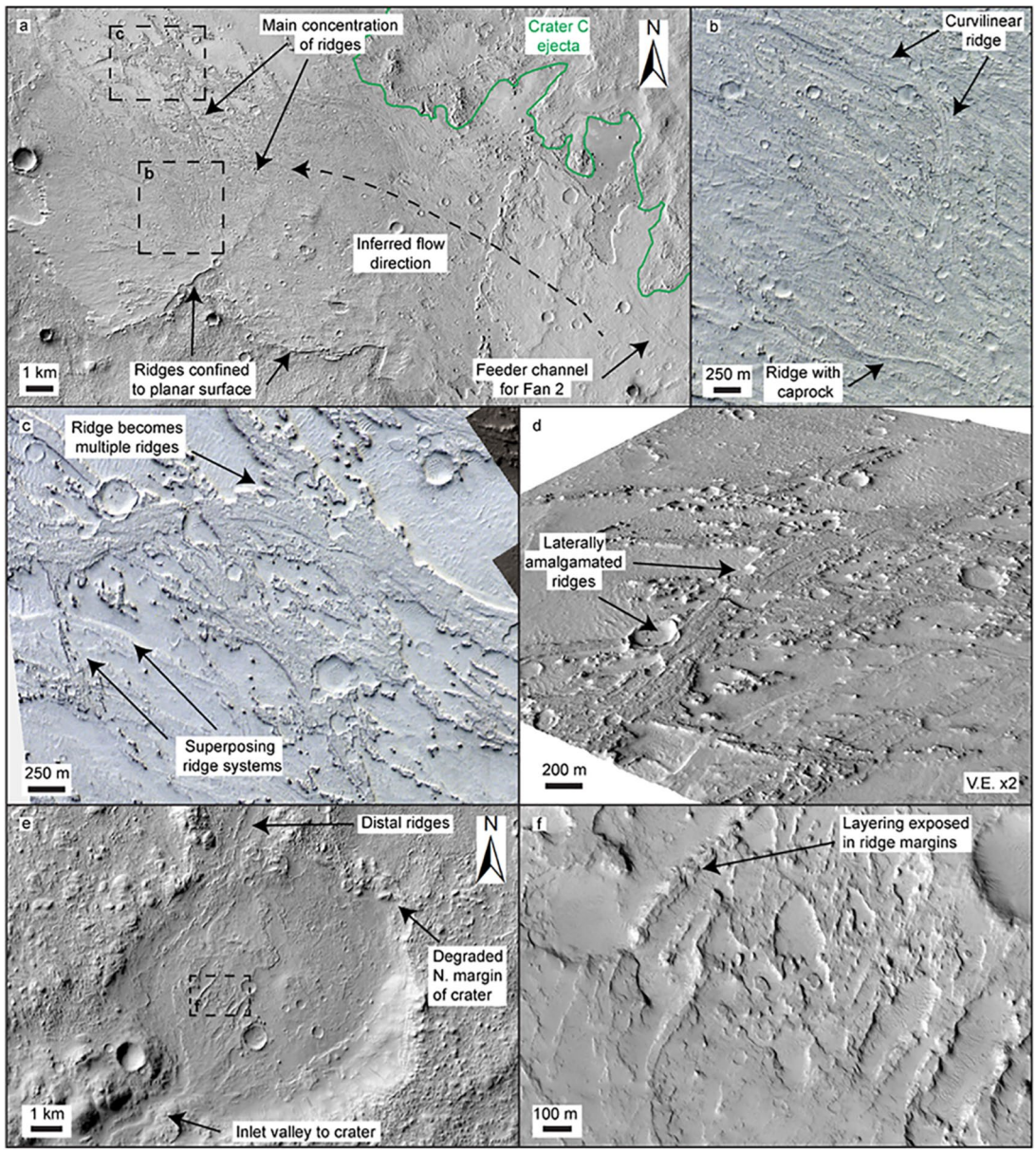

Figure 7. Fans 2 and 3. (a) CTX mosaic showing Fan 2, which occurs west of Crater C and originates from a feeder channel sourced at Unnamed Valley 1. (b) Section of Fan 2 showing curvilinear ridges, which show multiple orientations. (c) Section of Fan 2 showing superposing (stacked) and bifurcating ridge systems. Both (b) and (c) were constructed from a HiRISE image pansharpened with a PNB CaSSIS image. (d) Oblique view of Fan 2 facing northeast where multiple ridge systems have amalgamated together. View from constructed from HiRISE topography. (e) CTX mosaic showing Fan 3, which is found in a crater overlying the dichotomy. The northern margin of the crater has been eroded away. (f) HiRISE image showing section of Fan 3, which ridges are exposed.

meters (Figure 8b). The sediment bodies appear to be grouped into three branches (C-E), with Branch E being the stratigraphically youngest. On the top surfaces of the sediment bodies, erosion has exposed low relief, linear ridges, typically 50 m wide and <1 km long, which are orientated parallel to the long axis of the sediment bodies (Figure 8c). In some examples, the sediment bodies superpose one another. The sediment bodies broaden in the downslope direction (Figure 8d). These sediment bodies are being exhumed from within the surrounding terrain. Dividing the sediment bodies are negative relief channels, which are of generally similar dimensions. In total, from its apex to its most distal section, Fan 4 is ~20 km long and up to ~15 km wide. Overlying Fan 4 are erosional outliers of the MFF (Figure 8b).

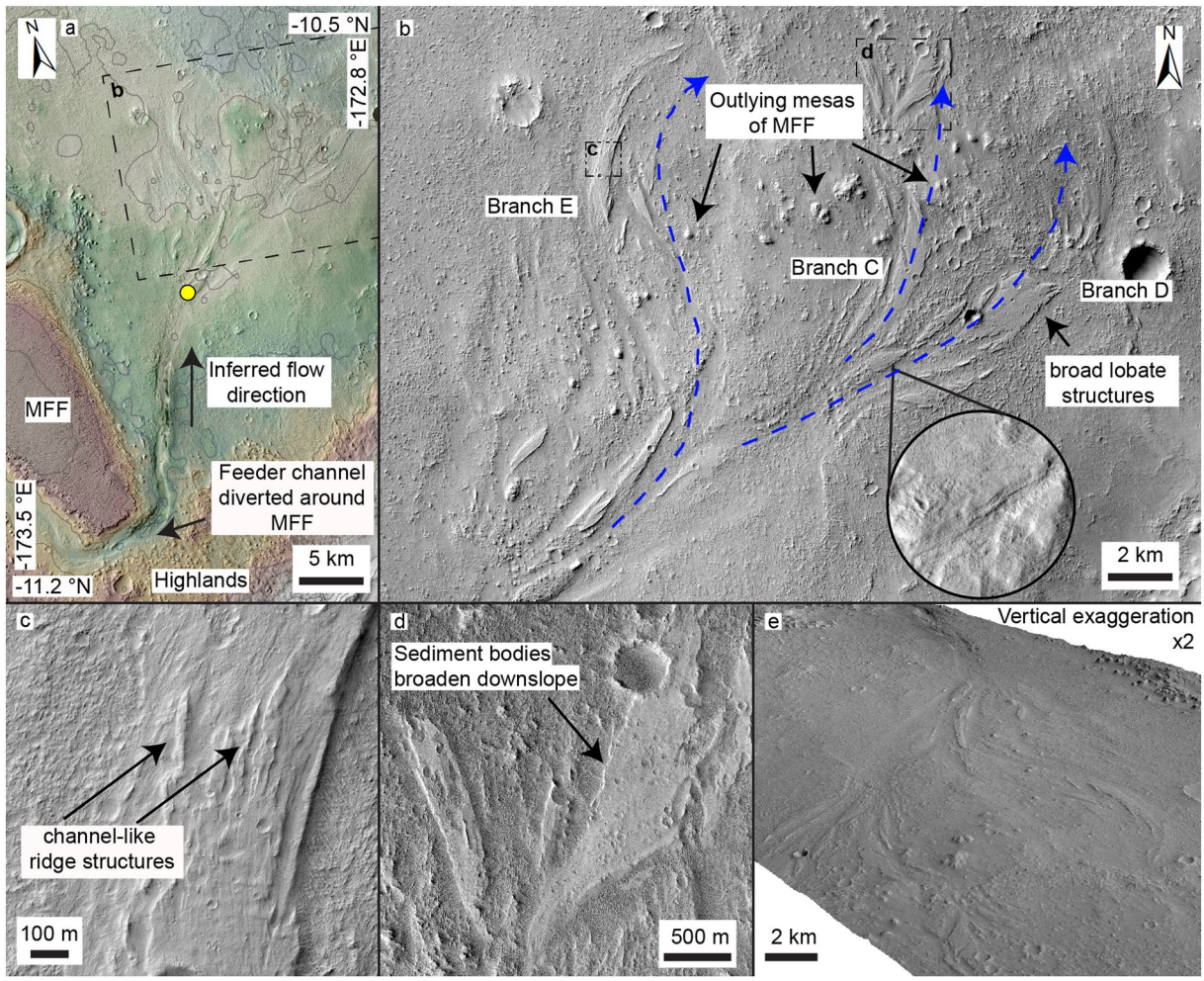

Figure 8. Fan 4. (a) MOLA topography overlaid on CTX mosaic showing Fan 4 (apex = yellow circle) and its feeder channel, which diverts around the MFF. (b) Mosaicked CTX image showing Fan 4, comprising elongated sediment bodies, which widen in the downslope direction. The sediment bodies are being exhumed from the surrounding terrain and are superposed by outliers of the MFF. Inset is HiRISE image showing layering exposed in margins of sediment bodies. (c) HiRISE image showing top surface of sediment bodies, where narrow, channel-like ridge structures are exposed. (d) HiRISE image showing sediment bodies near the downslope margin of Fan 4, which are wider than those further upslope. (e) Oblique view of Fan 4 facing upslope constructed from CTX topography.

Interpretation: Fan 4 is morphologically distinct from Fans 1–3. We interpret the low relief ridges on the sediment bodies as channel deposits which have amalgamated together. Although the sediment bodies broaden downslope, a clear channel-lobe transition is not observed, as seen in other martian sediment fans, interpreted as deltaic (e.g., Fawdon et al., 2018). Like previous examples, Fan 4 could plausibly be a fluvial or deltaic fan.

4.3.5. Fan 5

Observations: Fan 5 is outside the main study area but is relevant to understanding the evolution of MFF-dichotomy bound basin, as it occurs near its northeast margin (Figure 1b). Fan 5 begins at the dichotomy boundary at the end of a catchment at least 300 km long (Figure 1b). Fan 5 strongly differs from Fans 1–4 in its morphology: it comprises a series (at least three) of arcuate to lobate-shaped sedimentary deposits, which occur at discrete elevations and are interconnected by channels (Figure 9a). We term the three recognizable lobes, Lobes A-C. All three lobes have branching, distributary channels visible on their top surfaces. Lobe A, the most proximal lobe, is ~5 km long and forms at the dichotomy scarp, where the source bedrock valley network cross-cuts a wrinkle ridge and debouches into a shallow, degraded 4 km impact crater (Figure 9b). Lobe A is incised by a NNW orientated channel, which connects to Lobe B. Lobe B begins 10 km from the valley outlet and is 10 km

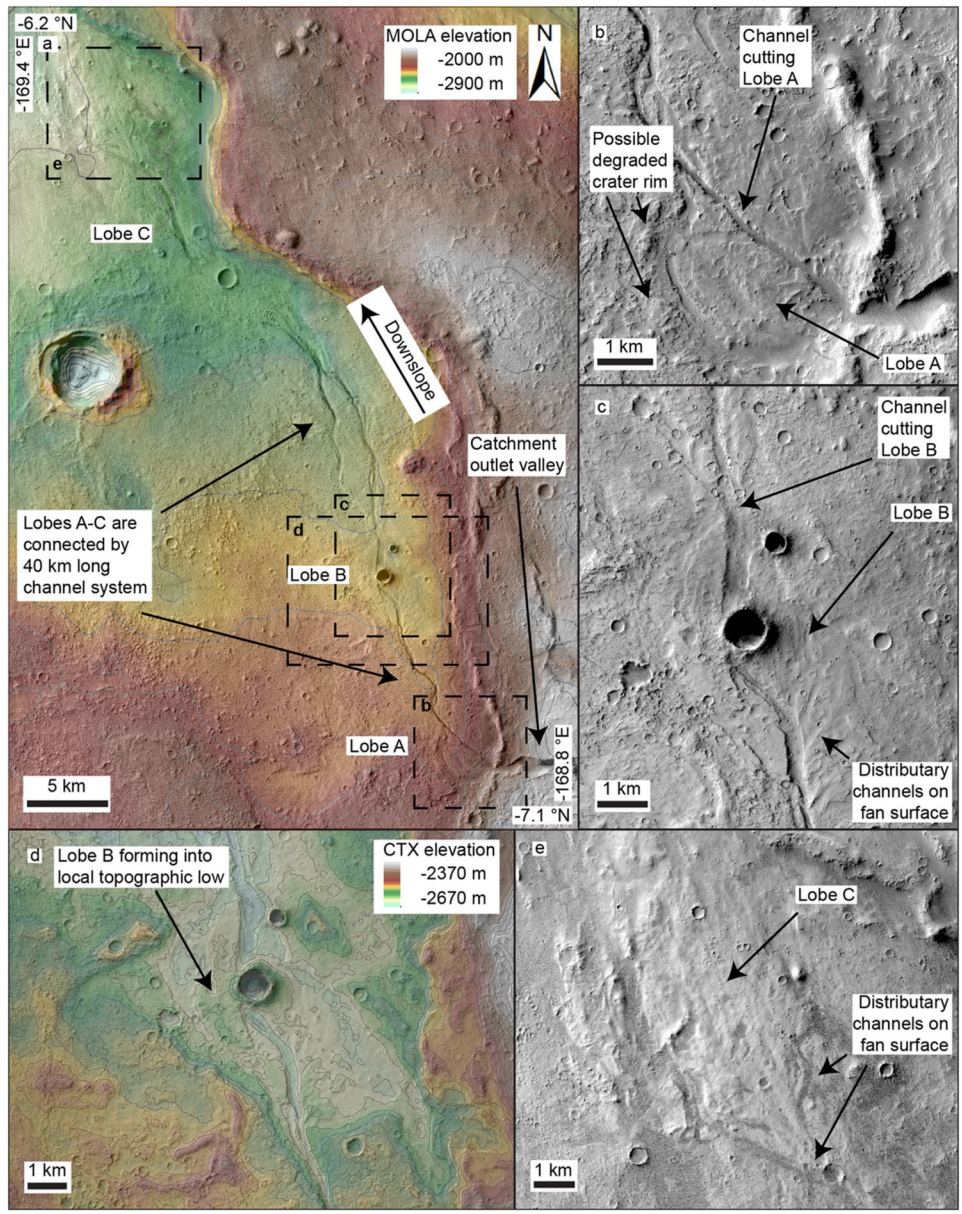

Figure 9. Fan 5. (a) MOLA topography overlaid on CTX mosaic showing Fan 5, which extends 40 km downslope from the valley outlet, forming three prominent lobes at discrete elevations. Lobe C is 200 m lower in elevation than Lobe A. (b) CTX image of the most proximal lobe, Lobe A, which formed into a degraded crater. (c) CTX image of Lobe B, downslope of Lobe A. (d) CTX topography and imagery showing that Lobe B appears to form into a local topographic low. Both Lobes A and B have been cut through by incisional channels. (e) CTX image of the most distal lobe, Lobe C, which is more poorly defined than the other lobes.

long (Figure 9c). Like Lobe A, Lobe B is set within a local topographic low, possibly a degraded impact crater (Figure 9d). At its northern margin, Lobe B has left the confines of this crater. Lobe B has subsequently been incised through by a channel, which has exposed sub-horizontal layering in its margins. The channel incising Lobe B connects to the most distal lobe, Lobe C. Lobe C (Figure 9e), begins 40 km NNW of the valley outlet and almost 200 m lower in elevation (Figure 9a). Lobe C forms into a topographically closed region of the MFF-dichotomy bound basin (rather than a local topographic low). Lobe C is approximately 12 km long and is not incised by subsequent channels.

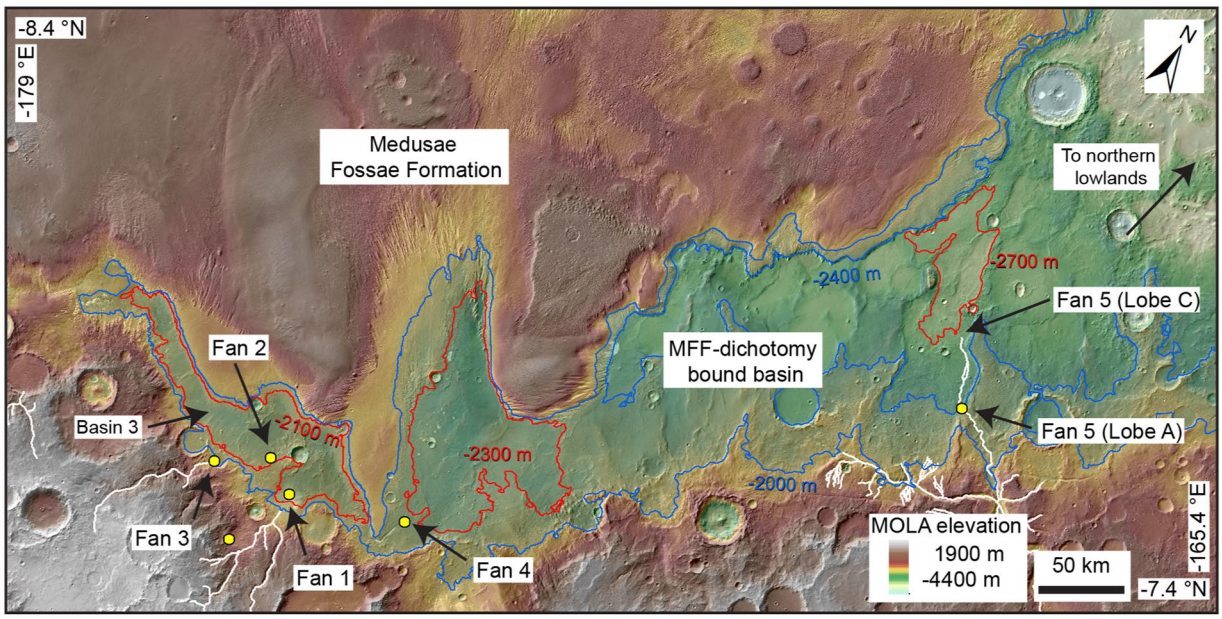

Figure 10. MOLA topography overlaid on THEMIS-IR day mosaic showing MFF-dichotomy bound basin. MOLA contours show which sediment fans which form at elevations that are topographically open (blue) or closed (red) to the northern lowlands. Fans 1, 2, 4 and 5 (Lobe C) form into locally closed basins, whereas Fans 2 and 5 (Lobe A) form at elevations open to the northern lowlands.

Interpretation: Fan 5 occurs over a much wider area than Fans 1–4, with distinct lobes separated by 200 m in elevation. The successive channels incising and connecting Lobes A-C suggest that each lobe is progressively younger (e.g., the channel cutting through and postdating Lobe A can be followed downslope to source Lobe B). The basinward-step of Fan 5 is consistent with both fluvial fans and delta bodies (e.g., Blum & Törnqvist, 2000).

4.4. Physiographic Setting of Downslope, MFF-Dichotomy Bound Basin

In this section, we describe the physiographic setting of the downslope, MFF-dichotomy bound basin and its relationship to the sediment fans (Figure 10). Above the −2,000 m contour, the basin is open to the northern lowlands, and encompasses the outlet of UV1. Fan 3 forms near this elevation (Figure 10). However, both Fans 1 and 2 form into a topographically closed basin defined by the −2,100 m contour, which we term Basin 3 (Figure 10). Similarly, Fan 4 forms into a topographically closed region of the main MFF-dichotomy bound basin, defined by the −2,300 m contour (Figure 10). To the east, Lobe A of Fan 5 forms close to the −2,400 m contour, which at this elevation is open to the lowlands (Figure 10). To contrast, Lobe C of Fan 5 forms into a topographically closed region defined by the −2,700 m contour (Figure 10).

5. Discussion

5.1. Incision, Filling, and Damming of the Catchment

In this section, we discuss the evolution of the catchment fluvial systems (UV1 and UV2). The presence of an inlet valley, an outlet, and terraces structures in Basin 1 supports an interpretation as an open paleolake basin (Figure 2; Fassett & Head, 2008; Goudge et al., 2012, 2016; Irwin et al., 2005; Ori et al., 2000). Additional open basin paleolakes may have existed further upslope, although these are poorly preserved (Figure 2). The evolution of the northern section of UV1 appears complex, with multiple stages of bedrock incision and sediment aggradation within the valley, in agreement with the multi-stage evolution interpreted by Irwin et al. (2005). Firstly, fluvial downcutting into bedrock must have occurred to form the initial valley. We estimate from CTX topography that incision was to a depth of up to 600–800 m, although the original valley walls are so poorly preserved that this is difficult to determine. Bedrock strath terraces along UV1 and in Basin 1 indicates that multiple periods of downcutting may have occurred (Figure 3). The course of UV1 appears to have been controlled by the topography generated by impact craters and their ejecta along the valley margins (Figure 3a). UV1 is not

graded to an equilibrium profile (Figure 2b), indicating that it was an immature fluvial system, like many other examples across Mars (e.g., Fassett & Head, 2008; Goudge & Fassett, 2018; Hynek et al., 2010).

The valley floor of UV1 has been filled by sediment to an unknown depth (we estimate at least several hundred meters; Figure 3). The fill may be due to impact cratering, input from the MFF, or channel-fill associated with the fluvial system itself. Regardless of its origin, incision into the fill in two distinct regions (I1 and I2) indicates that the fill was later modified by subsequent fluvial processes (Figures 3b and 3c). I1 (Figure 3b) begins at the outlet of Basin 1, so the incision may have been caused by an overflow flooding event from the lake which occupied Basin 1 (Goudge & Fassett, 2018). We note that overflow flooding cannot be responsible for the downcutting which originally formed UV1 as the original valley walls exceed the maximum elevation of the walls of B1. I1 shallows in the downslope direction (from 300 m to 0) and it eventually becomes buried by Crater A.

The reason for the formation of I2 (Figure 3c), at a prominent knickpoint north of Crater A, is unclear. Knickpoints may be caused by lithologic variation in the underlying bedrock of the incised valley, when a material that is resistant to erosion is encountered (e.g., Gilbert, 1896). As the resistant layer is eroded, the knickpoint migrates upstream. Knickpoint formation may also have been initiated by base level fall within a downstream body of water, concentrating incision in the downslope region of UV1 (e.g., Goudge & Fassett, 2018; Howard, 1994). Near the dichotomy boundary, I2 has been buried by the ejecta from Crater B (Figure 4a). However, the ejecta from Crater B has subsequently been incised, indicating that the formation of Crater B was syn-fluvial, temporarily damming UV1, or that Crater B formed in between periods of fluvial activity. In either scenario, UV1/I2 later incised through the ejecta from Crater B. South of Crater B, the inferred flow directions of UV2 indicate that it may have originally been a tributary of UV1. Following the formation of Crater B, its ejecta formed a dam and UV2 was likely diverted SW into Basin 2 (Figure 4b), where water may have pooled, forming a paleolake.

The inverted channel deposits in the downslope regions of UV1 and UV2 indicates the presence of channel-fill and net deposition within the valleys (Figures 4a and 4c). Inverted channel deposits bound within the downslope region of erosional valleys are observed elsewhere on Mars (Dickson et al., 2021), notably Arabia Terra, where they are often found in proximity to paleolake basins (Davis et al., 2016, 2019). In filled valley sequences on Earth, these processes can be driven by changes in base level, or water or sediment supply (e.g., Blum & Aslan, 2006; Singh et al., 2017). The proximity to the downslope MFF-dichotomy bound basin (if it contained water) opens the possibility that these regions of UV1 and UV2 were subject to the effects of water level fluctuations (Blum et al., 2013). Stratigraphic relationships indicate that the formation of these inverted channel deposits likely postdates the formation of Crater B. Thus, this association indicates that the formation of Crater B may be responsible for the aggradation within both UV1 and UV2, potentially by supplying ample unconsolidated sediment to the system or causing a local rise in base level. The formation of Crater A, which superposes both UV1 and UV2, and whose ejecta does not appear incised, seemingly occurred after the cessation of fluvial activity within the catchment.

5.2. Formation of the Sediment Fans

In this section, we interpret sediment fans and consider their formation environment. Many fans appear dominated by ridges (Figures 6 and 7) or sediment bodies which erode into ridges (Figure 8), which we have interpreted as inverted channel systems. The stacked nature of the ridges (Figures 6, 7c, and 7d) and the amalgamation of multiple ridges (Figures 6, 7d, and 8) supports an interpretation as exhumed channel-belt deposits, rather than the inversion of single-fill channels (DiBiase et al., 2013; Hayden et al., 2019; Martinez et al., 2010). Ridges within Fans 1, 2 and 4 occur in stratigraphically and topographically separated branches (Figures 6–8), suggesting that these fans built up multiple, laterally stacked sedimentary deposits, formed by the avulsion and aggradation of river channels (e.g., Balme et al., 2020; Davis et al., 2019). Within the stratigraphically distinct branches of Fan 1, bifurcation nodes are exposed at different elevations (Figure 6), suggesting that Fan 1 may have grown out basinward over time, possibly in response to changing downslope water levels (e.g., Fawdon et al., 2018).

Fans 1, 2 and 4 are all set within low relief plains and do not occur at topographic escarpments, unlike alluvial fans (Blair & McPherson, 1994), and are more consistent with fluvial fans or deltas (Ventra & Clarke, 2018). Fans 1, 2 and 4 all form into topographically closed basins, within or adjacent to the main MFF-dichotomy bound basin (Figure 10), suggesting the fans delivered water to these regions. The planform pattern, progressive bifurcations, and digitate ridge terminations, best exposed in Fan 1, although sometimes visible in Fan 2, are similar

to other exhumed sediment fan deposits on Mars, interpreted as deltas forming into water bodies, such as those in Eberswalde crater (e.g., Rice et al., 2013), Aeolis Dorsa (e.g., DiBiase et al., 2013), Jezero crater (e.g., Goudge et al., 2017), and SW Melas (e.g., Davis et al., 2018; Williams & Weitz, 2014).

To contrast, Fans 3 (Figures 7e and 7f) and 5 are defined by lobate-shaped deposits (Figure 9). Although Fan 3 forms near an elevation contour open to the lowlands (Figure 10), the majority of Fan 3 is confined to its hosting impact crater (Figures 7e and 7f), suggesting it formed into a lake confined to the crater (e.g., Fassett & Head, 2008), rather than a more expansive basin. The distal inverted channel deposits on Fan 3 and the degraded state of the northern crater margin, point to deposition eventually leaving the confines of the crater.

Similarly, although Lobes A and B of Fan 5 occurs near an elevation open to the northern lowlands (Figure 10), we note these deposits form into local topographic lows (e.g., craters; Figure 9) not apparent in MOLA topography, suggesting that sediment deposition infilled local accommodation (i.e., impact craters), rather than a wider basin. These observations are generally more consistent with the behavior of a fluvial fan than a delta. The 40 km progression in downslope lobe formation indicates a downstream migration in sediment deposition over time, which was concentrated in local topographic lows. Lobes A and B are successively incised by channels, with the new lobe deposition occurring downslope of the incised channel, possibly driven by reduction in sediment supply or lowering of base level (e.g., Blum & Törnqvist, 2000). The terminal lobe, Lobe C, forms into a wider basin (Figure 10), and it is conceivable that a larger body of water may have pooled here (although not filling the main MFF-dichotomy bound basin). In summary, all five fans are generally consistent with distributary channel and sediment fan systems, and there is tentative evidence at least some of them may have formed in water bodies.

5.3. Chronology of the Fluvial Systems

In this section, we consider when the fluvial systems were active to place them into broader context. UV1, UV2, and other nearby valley networks incise into mid Noachian age terrain (~3.9–3.8 Ga; Tanaka et al., 2014), which places an upper bracket on their formation. We note that the original valley walls are highly degraded (Figures 2 and 3), so it is possible that the valley fill, inverted channel systems and sediment fans are significantly younger. Fans 1, 2, 4 and 5 all form onto terrain mapped as early Hesperian (~3.7–3.5 Ga; Tanaka et al., 2014) in age. The age of the adjacent MFF is difficult to determine as its extreme friability limits conventional crater counting techniques. Kerber and Head (2010) analyzed the stratigraphic relationship of the MFF to lava flows and impact craters to determine its emplacement age. Kerber and Head (2010) suggest that in this region, the MFF (Lucus Planum) was emplaced during the Hesperian. The feeder channel for Fan 4 is clearly diverted around, and infilled by, the MFF, and Fan 4 itself is overlain by erosional outliers of the MFF (Figure 8). These observations suggest that the MFF was at least partially emplaced before the formation of Fan 4 and that its formation continued afterward. Significant volumes of sediment may have been supplied to the fluvial systems if they were coeval with the emplacement of the MFF (i.e., volcaniclastic).

The feeder channel for Fan 4 may have been sourced from overspill from Basin 3 (which hosted Fans 1 and 2; Figure 10), although we cannot exclude the possibility that these systems were active at different times. As Crater A superposes UV1 and it is not incised, its formation at 3.5 Ga (Figure 5) likely represents a lower age bracket for the cessation of fluvial processes. Fans 1, 2 and 3 were likely fed by UV1 and its associated valley networks, also putting a bracket on their activity. It is possible that some fluvial systems were locally reactivated by late-stage flows, as seen elsewhere on Mars (e.g., Bouley et al., 2009). In summary, we conclude that fluvial processes were likely active between the mid-Noachian and early Hesperian (3.9–3.5 Ga), although most landforms described here probably represent the younger part of this age bracket.

5.4. Nature and Evolution of the Downslope Basin

In this section, we consider the environment of the downslope basin (Figure 1), bound by the MFF and the dichotomy scarp, in particular relation to the existence of an ancient ocean. We consider five possible scenarios for the evolution of this basin:

1. The fluvial systems predate the MFF and thus the basin did not exist at the time they were forming
2. The fluvial systems formed into an entirely dry, sub-aerial basin
3. The fluvial systems formed into a large, sub-aqueous basin, which was disconnected or

4. Connected to a water body in the northern lowlands
5. The MFF-dichotomy basin was mostly dry, but the fluvial systems formed in localized paleolake basins

The stratigraphic relationship of the MFF to Fan 4 (Figure 8) rules out scenario 1. There is tentative evidence that at least some of the fans may have formed into water bodies, making scenario 2 less likely, although we cannot rule it out entirely. Some of the fans do form near the dichotomy equipotential level defined by Di Achille and Hynek (2010): ~−2,500 m. However, we note that the fans all form at distinct elevations (separated by up to 700 m), either into closed sub-basins within the main MFF-dichotomy bound basin (Figure 10), or into local topographic lows (i.e., impact craters). Unlike other sediment fans identified along the dichotomy (Di Achille & Hynek, 2010), the fans in this region do not form an equipotential surface. It therefore seems unlikely that the fluvial systems, as they are currently expressed, formed into a large, sub-aqueous basin, that was either disconnected or connected to the northern lowlands (scenarios 3 and 4).

Instead, the morphology and physiography of the fluvial systems suggests that at least some of the sediment fans formed into local paleolake basins, set within the wider MFF-dichotomy bound basin (scenario 5). It is conceivable that the lake basin hosting Fans 1 and 2 (Basin 3) was connected to the basin hosting Fan 4 (Figure 10). The paleolake basins which the sediment fans form into could represent the last stages of a large, drying body of water. The basinward growth of Fan 1 (Figure 6) may record this drying, however, the changes to Fan 1 are much smaller and more localized than those observed elsewhere along the dichotomy, such as Aeolis Dorsa (e.g., Cardenas et al., 2017; Hughes et al., 2019) or Hypanis Valles (e.g., Fawdon et al., 2018). Fan 5 also shows evidence for basinward growth, however, Lobes A and B form into successive local topographic lows, suggesting that deposition shifted basinwards once the local accommodation was filled, rather than being driven by a larger water body that receded.

Our results agree with previous studies of the dichotomy boundary in the Gale crater region (García-Arnay & Gutiérrez, 2020; Rivera-Hernández & Palucis, 2019), in which sediment fans were characterized as forming into a series of paleolake basins, rather than a hemisphere-spanning ocean. We note that the Memnonia Sulci systems were likely active at a similar time to the Hypanis Valles and Gale crater region systems (Noachian to early Hesperian; García-Arnay & Gutiérrez, 2020; Fawdon et al., 2018). Additionally, our results generally agree with a recent global-scale investigation which demonstrated that the sediment fans along the dichotomy mostly do not have the spatial-temporal relationships to indicate they formed into a hemisphere-spanning ocean where the water levels were changing (De Toffoli et al., 2021).

6. Conclusions

We used high-resolution image and topographic datasets to investigate valley networks, paleolake basins, inverted channel systems, and sediment fans in the NW Memnonia Sulci region of Mars. The extensive upslope catchment comprises highly degraded valley networks, which reveal a complex evolutionary history including multiple periods of incision and filling. The fluvial catchment has been influenced by overflow floods from upslope basins and impact crater damming, leading to the diversion of flows and aggradation within the catchment. The catchment also shows some evidence for the influence of a downslope body of water. Downslope, a series of sediment form into a large basin, bound by the topographic dichotomy and Medusae Fosse Formation. The morphology of the sediment fans is generally consistent with a formation as fluvial fans or deltas. The physiographic setting of the fans suggests they formed into a series of paleolake basins, situated on the margins of the dichotomy, rather than a large regional water body or ocean, although it is unclear if a more extensive water body may have existed earlier. Stratigraphic relationships and crater counts suggest that fluvial activity likely occurred between the mid Noachian and early Hesperian. Our results (a) demonstrate the complex, multi-phase evolution of fluvial systems on ancient Mars (e.g., Edgett et al., 2020) and (b) highlight the importance of regional studies when assessing the nature of the northern lowlands basin on early Mars, which can differ from the global picture.

Data Availability Statement

The standard data products used here are available from the NASA Planetary Data System as follows. (1) HiRISE: https://hirise-pds.lpl.arizona.edu/PDS/; (McEwen, 2006). (2) CTX: https://pds-imaging.jpl.nasa.gov/volumes/mro.html; (Malin, 2007). (3) THEMIS: https://pds-imaging.jpl.nasa.gov/volumes/ody.html; (Edwards

et al., 2011). (4) MOLA: https://pds-geosciences.wustl.edu/missions/mgs/megdr.html; (Neumann et al., 2003). CaSSIS data are available through the ESA Planetary Science Archive (http://archives.esac.esa.int/psa/#!Table%20View/CaSSIS=instrument). CTX and HiRISE Digital Elevation Models, shapefiles, and CraterStats2 files created for this project are available in the Figshare archive: https://doi.org/10.6084/m9.figshare.c.5501313.v1; (Davis, 2021).

Acknowledgments
Support from the UK Space Agency is gratefully acknowledged (JMD: ST/R002355/1; ST/V002678/1; ST/W002566/1, PF: ST/R001413/1; ST/W002736/1). LA was supported by an Undergraduate Research Opportunities Programme bursary from Imperial College London. PF acknowledges support from the Open University Space Strategic Research Area. We thank the various Mars instrument science and engineering teams for their consistent and dedicated work. We thank two anonymous reviewers for thorough and constructive reviews. CaSSIS is a project of the University of Bern and funded through the Swiss Space Office via ESA's PRODEX programme. The instrument hardware development was also supported by the Italian Space Agency (ASI; ASI-INAF agreement no. I/018/12/0), INAF/Astronomical Observatory of Padova, and the Space Research Center (CBK) in Warsaw. Support from SGF (Budapest), the University of Arizona (Lunar and Planetary Lab.) and NASA are also gratefully acknowledged. Operations support from the UK Space Agency under grant ST/R003025/1 is also acknowledged.

References

Adler, J. B., Bell, J. F., III, Fawdon, P., Davis, J., Warner, N. H., Sefton-Nash, E., & Harrison, T. N. (2019). Hypotheses for the origin of the Hypanis fan-shaped deposit at the edge of the Chryse escarpment, Mars: Is it a delta? *Icarus*, *319*, 885–908. https://doi.org/10.1016/j.icarus.2018.05.021

Alemanno, G., Orofino, V., & Mancarella, F. (2018). Global map of Martian fluvial systems: Age and total eroded volume estimations. *Earth and Space Science*, *5*, 560–577. https://doi.org/10.1029/2018EA000362

Balme, M. R., Gupta, S., Davis, J. M., Fawdon, P., Grindrod, P. M., Bridges, J. C., et al. (2020). Aram dorsum: An extensive mid-noachian age fluvial depositional system in Arabia Terra, Mars. *Journal of Geophysical Reseach: Planets*, *125*, e2019JE006244. https://doi.org/10.1029/2019JE006244

Barlow, N. G., Boyce, J. M., Costard, F. M., Craddock, R. A., Garvin, J. B., Sakimoto, S. E. H., et al. (2000). Standardizing the nomenclature of Martian impact crater ejecta morphologies. *Journal of Geophysical Research: Planets*, *105*(E11), 26733–26738. https://doi.org/10.1029/2000JE001258

Bibring, J.-P., Langevin, Y., Mustard, J. F., Poulet, F., Arvidson, R., Gendrin, A., et al. (2006). Global mineralogical and aqueous mars history derived from OMEGA/Mars Express data. *Science*, *312*(5772), 400–404. https://doi.org/10.1126/science.1122659

Blair, T. C., & McPherson, J. G. (1994). *Alluvial fan processes and forms: Geomorphology of desert environments* (pp. 354–366). https://doi.org/10.1007/978-94-015-8254-4_14

Blum, M., & Aslan, A. (2006). Signatures of climate vs. sea-level change within incised valley-fill successions: Quaternary examples from the Texas Gulf Coast. *Sedimentary Geology*, *190*, 177–211. https://doi.org/10.1016/j.sedgeo.2006.05.024

Blum, M., Martin, J., Milliken, K., & Garvin, M. (2013). Paleovalley systems: Insights from Quaternary analogs and experiments. *Earth-Science Reviews*, *116*, 128–169. https://doi.org/10.1016/j.earscirev.2012.09.003

Blum, M. D., & Törnqvist, T. E. (2000). Fluvial responses to climate and sea-level change: A review and look forward. *Sedimentology*, *47*(SUPPL. 1), 2–48. https://doi.org/10.1046/j.1365-3091.2000.00008.x

Bouley, S., Ansan, V., Mangold, N., Masson, P., & Neukum, G. (2009). Fluvial morphology of Naktong Vallis, Mars: A late activity with multiple processes. *Planetary and Space Science*, *57*(8-9), 982–999. https://doi.org/10.1016/j.pss.2009.01.015

Burr, D. M., Williams, R. M. E., Wendell, K. D., Chojnacki, M., & Emery, J. P. (2010). Inverted fluvial features in the Aeolis/Zephyria Plana region, Mars: Formation mechanism and initial paleodischarge estimates. *Journal of Geophysical Research*, *115*, E07011. https://doi.org/10.1029/2009JE003496

Cardenas, B. T., Mohrig, D., & Goudge, T. A. (2017). Fluvial stratigraphy of valley fills at Aeolis Dorsa, Mars: Evidence for base-level fluctuations controlled by a downstream water body. *The Geological Society of America Bulletin*, *130*, 484–498. https://doi.org/10.1130/B31567.1

Carr, M. H., & Head, J. W., III (2003). Oceans on Mars: An assessment of the observational evidence and possible fate. *Journal of Geophysical Research*, *108*(E5), 5042. https://doi.org/10.1029/2002JE001963

Christensen, P. R., Jakosky, B. M., Kieffer, H. H., Malin, M. C., McSween, H. Y., Jr., Nealson, K., et al. (2004). The thermal emission imaging system (THEMIS) for the Mars 2001 Odyssey mission. *Space Science Reviews*, *110*, 85–130. https://doi.org/10.1023/b:spac.0000021008.16305.94

Citron, R. I., Manga, M., & Hemingway, D. J. (2018). Timing of oceans on Mars from shoreline deformation. *Nature*, *555*, 643–646. https://doi.org/10.1038/nature26144

Clifford, S. M., & Parker, T. J. (2001). The evolution of the Martian hydrosphere: Implications for the fate of a primordial ocean and the current state of the northern plains. *Icarus*, *154*, 40–79.

Craddock, R. A., & Howard, A. D. (2002). The case for rainfall on a warm, wet early Mars. *Journal of Geophysical Research*, *107*, E11. https://doi.org/10.1029/2001JE001505

Craddock, R. A., Maxwell, T. A., & Howard, A. D. (1997). Crater morphometry and modification in the Sinus Sabaeus and margaritifer Sinus regions of Mars. *Journal of Geophysical Research*, *102*, 13321–13340. https://doi.org/10.1029/97JE01084

Davis, J. M., Balme, M., Grindrod, P. M., Williams, R. M. E., & Gupta, S. (2016). Extensive noachian fluvial systems in Arabia Terra: Implications for early Martian climate. *Geology*, *44*, 847–850. https://doi.org/10.1130/G38247.1

Davis, J. (2021). *CTX and HiRISE digital elevation models - Memnonia Sucli, Mars*. figshare. Collection. https://doi.org/10.6084/m9.figshare.c.5501313.v1

Davis, J. M., Grindrod, P. M., Banham, S. G., Warner, N. H., Conway, S. J., Bozman, S. J., & Gupta, S. (2021). A record of syn-tectonic sedimentation revealed by perched alluvial fan deposits in Valles Marineris, Mars. *Geology*, *49*. https://doi.org/10.1130/G48971.1. v. in press.

Davis, J. M., Grindrod, P. M., Fawdon, P., Williams, R. M. E., Gupta, S., & Balme, M. (2018). Episodic and declining fluvial processing in southwest Melas chasma, Valles marineris, Mars. *Journal of Geophysical Research*, *123*, 2527–2549. https://doi.org/10.1029/2018JE005710

Davis, J. M., Gupta, S., Balme, M., Grindrod, P. M., Fawdon, P., Dickeson, Z. I., & Williams, R. M. E. (2019). A diverse array of fluvial depositional systems in Arabia Terra: Evidence for mid-noachian to early Hesperian rivers on Mars. *Journal of Geophysical Research: Planets*, *124*, 1913–1934. https://doi.org/10.1029/2019JE005976

De Toffoli, B., Plesa, A.-C., Hauber, E., & Breuer, D. (2021). Delta deposits on Mars: A global perspective. *Geophysical Research Letters*, *48*, e2021GL094271. https://doi.org/10.1029/2021GL094271

Di Achille, G., & Hynek, B. M. (2010). Ancient ocean on Mars supported by global distribution of deltas and valleys. *Nature Geoscience*, *3*, 459–463. https://doi.org/10.1038/ngeo891

DiBiase, R. A., Limaye, A. B., Scheingross, J. S., Fischer, W. W., & Lamb, M. P. (2013). Deltaic deposits at Aeolis Dorsa: Sedimentary evidence for a standing body of water on the northern plains of Mars. *Journal of Geophysical Research: Planets*, *118*, 1285–1302. https://doi.org/10.1002/jgre.20100

Dickeson, Z. I., & Davis, J. M. (2020). Martian oceans. *Astronomy and Geophysics*, *61*, 3.11–3.17. https://doi.org/10.1093/astrogeo/ataa038

Dickson, J. L., Lamb, M. P., Williams, R. M. E., Hayden, A. T., & Fischer, W. W. (2021). The global distribution of depositional rivers on early Mars. *Geology*, *49*, 504–509. https://doi.org/10.1130/G48457.1

Edgett, K. S., Banham, S. G., Bennett, K. A., Edgar, L. A., Edwards, C. S., Fairén, A. G., et al. (2020). Extraformational sediment recycling on Mars: Geosphere. *Geosphere*, *16*(6), 1508–1537. https://doi.org/10.1130/GES02244.1

Edwards, C. S., Nowicki, K. J., Christensen, P. R., Hill, J., Gorelick, N., & Murray, K. (2011). Mosaicking of global planetary image datasets: 1. Techniques and data processing for Thermal Emission Imaging System (THEMIS) multi-spectral data. *Journal of Geophysical Research*, *116*, E10008. https://doi.org/10.1029/2010JE003755

Ehlmann, B. L., & Edwards, C. S. (2014). Mineralogy of the martian surface. *Annual Review of Earth and Planetary Sciences*, *42*(1), 291–315. https://doi.org/10.1146/annurev-earth-060313-055024

Fassett, C. I., & Head, J. W. (2008). Valley network-fed, open-basin lakes on Mars: Distribution and implications for Noachian surface and subsurface hydrology. *Icarus*, *198*, 37–56. https://doi.org/10.1016/j.icarus.2008.06.016

Fawdon, P., Gupta, S., Davis, J. M., Warner, N. H., Adler, J. B., Balme, M., et al. (2018). The Hypanis Valles delta: The last highstand of a sea on early Mars? *Earth and Planetary Science Letters*, *500*, 225–241. https://doi.org/10.1016/j.epsl.2018.07.040

Ganti, V., Chu, Z., Lamb, M. P., Nittrouer, J. A., & Parker, G. (2014). Testing morphodynamic controls on the location and frequency of river avulsions on fans versus deltas: Huanghe (Yellow River), China. *Geophysical Research Letters*, *41*, 7882–7890. https://doi.org/10.1002/2014GL061918

García-Arnay, Á., & Gutiérrez, F. (2020). Reconstructing paleolakes in Nepenthes Mensae, Mars, using the distribution of putative deltas, coastal-like features, and terrestrial analogs. *Geomorphology*, *359*, 107129. https://doi.org/10.1016/j.geomorph.2020.107129

Gilbert, G. K. (1896). Niagara Falls and their history. In J. W. Powell (Ed.), *The physiography of the United States: Ten monographs, national geographic society* (pp. 203–236). American Book Company.

Goudge, T. A., & Fassett, C. I. (2018). Incision of Licus Vallis, Mars, from multiple lake overflow floods. *Journal of Geophysical Research Planets*, *123*, 405–420. https://doi.org/10.1002/2017JE005438

Goudge, T. A., Head, J. W., Mustard, J. F., & Fassett, C. I. (2012). An analysis of open-basin lake deposits on Mars: Evidence for the nature of associated lacustrine deposits and post-lacustrine modification processes. *Icarus*, *219*, 211–229. https://doi.org/10.1016/j.icarus.2012.02.027

Goudge, T. A., Milliken, R. E., Head, J. W., Mustard, J. F., & Fassett, C. I. (2016). Sedimentological evidence for a deltaic origin of the western fan deposit in Jezero crater, Mars and implications for future exploration. *Earth and Planetary Science Letters*, *1*, 1–9. https://doi.org/10.1016/j.epsl.2016.10.056

Goudge, T. A., Milliken, R. E., Head, J. W., Mustard, J. F., & Fassett, C. I. (2017). Sedimentological evidence for a deltaic origin of the western fan deposit in Jezero crater, Mars and implications for future exploration. *Earth and Planetary Science Letters*, *458*, 357–365. https://doi.org/10.1016/j.epsl.2016.10.056

Grotzinger, J. P., Gupta, S., Malin, M. C., Rubin, D. M., Schieber, J., Siebach, K., et al. (2015). Deposition, exhumation, and paleoclimate of an ancient lake deposit, Gale crater, Mars. *Science*, *350*(6257), aac7575–aac7571. https://doi.org/10.1126/science.aac7575

Hartmann, W. K., & Neukum, G. (2001). Cratering chronology and the evolution of Mars. *Space Science Reviews*, *96*, 165–194. https://doi.org/10.1023/A:1011945222010

Hayden, A. T., Lamb, M. P., Fischer, W. W., Ewing, R. C., McElory, B. J., & Williams, R. M. E. (2019). Formation of sinuous ridges by inversion of river-channel belts in Utah, USA, with implications for Mars. *Icarus*. https://doi.org/10.1016/j.icarus.2019.04.019

Howard, A. D. (1994). A detachment-limited model of drainage basin evolution. *Water Resources Research*, *30*, 2261–2285.

Howard, A. D., Moore, J. M., & Irwin, R. P. (2005). An intense terminal epoch of widespread fluvial activity on early Mars: 1. Valley network incision and associated deposits. *Journal of Geophysical Research*, *110*, E12S14. https://doi.org/10.1029/2005JE002459

Hughes, C. M., Cardenas, B. T., Goudge, T. A., & Mohrig, D. (2019). Deltaic deposits indicative of a paleo-coastline at Aeolis Dorsa, Mars. *Icarus*, *317*, 442–453. https://doi.org/10.1016/j.icarus.2018.08.009

Hynek, B. M., Beach, M., & Hoke, M. R. T. (2010). Updated global map of Martian valley networks and implications for climate and hydrologic processes. *Journal of Geophysical Research*, *115*, E09008. https://doi.org/10.1029/2009JE003548

Irwin, R. P., & Howard, A. D. (2002). Drainage basin evolution in noachian Terra cimmeria, Mars. *Journal of Geophysical Research*, *107*, E75056. https://doi.org/10.1029/2001JE001818

Irwin, R. P., Howard, A. D., Craddock, R. A., & Moore, J. M. (2005). An intense terminal epoch of widespread fluvial activity on early Mars: 2. Increased runoff and paleolake development. *Journal of Geophysical Research*, *110*, E12S15. https://doi.org/10.1029/2005JE002460

Ivanov, B. A. (2001). Mars/Moon cratering rate ratio estimates. *Space Science Reviews*, *96*, 87–104. https://doi.org/10.1023/A:1011941121102

Kerber, L., & Head, J. W. (2010). The age of the Medusae Fossae Formation: Evidence of Hesperian emplacement from crater morphology, stratigraphy, and ancient lava contacts. *Icarus*, *206*(2), 669–684. https://doi.org/10.1016/j.icarus.2009.10.001

Kirk, R. L., Howington-Kraus, E., Rosiek, M. R., Anderson, J. A., Archinal, B. A., Becker, K. J., et al. (2008). Ultrahigh resolution topographic mapping of Mars with MRO HiRISE stereo images: Meter-scale slopes of candidate Phoenix landing sites. *Journal of Geophysical Research*, *113*, E00A24. https://doi.org/10.1029/2007JE003000

Kneissl, T., van Gasselt, S., & Neukum, G. (2011). Map-projection-independent crater size-frequency determination in GIS environments—New software tool for ArcGIS. *Planetary and Space Science*, *59*, 1243–1254. https://doi.org/10.1016/j.pss.2010.03.015

Lefort, A., Burr, D. M., Beyer, R. A., & Howard, A. D. (2012). Inverted fluvial features in the aeolis-zephyria plana, western Medusae Fossae Formation, Mars: Evidence for post-formation modification. *Journal of Geophysical Research*, *117*, E03007. https://doi.org/10.1029/2011je004008

Malin, M. C. (2007). MRO Context Camera experiment data record level 0 v1.0. [Data set]. NASA Planetary Data System. https://doi.org/10.17189/1520266

Malin, M. C., Bell, J. F., III, Cantor, B. A., Caplinger, M. A., Calvin, W. M., Clancy, R. T., et al. (2007). Context Camera investigation on board the Mars reconnaissance orbiter. *Journal of Geophysical Research*, *112*, E05S04. https://doi.org/10.1029/2006JE002808

Mandt, K. E., de Silva, S. L., Zimbelman, J. R., & Crown, D. A. (2008). Origin of the Medusae Fossae Formation, Mars: Insights from a synoptic approach. *Journal of Geophysical: Research Planets*, *113*(12). https://doi.org/10.1029/2008JE003076

Martinez, J. L. C., Perez, L. C., Marcuello, A., Cazo, P. A., Carpio, M. M., & Bellmunt, F. (2010). exhumed channel sandstone networks within fluvial fan deposits from the oligo-miocene caspe formation, south-east ebro Basin (North-east Spain). *Sedimentology*, *57*(1), 162–189. https://doi.org/10.1111/j.1365-3091.2009.01096.x

McEwen, A. S. (2006). MRO Mars High Resolution Image Science Experiment RDR V1.0. [Data set]. NASA Planetary Data System. https://doi.org/10.17189/1520303

McEwen, A. S., Eliason, E. M., Bergstrom, J. W., Bridges, N. T., Hansen, C. J., Delamere, W. A., et al. (2007). Mars reconnaissance orbiter's high resolution imaging science experiment (HiRISE). *Journal of Geophysical Research*, *112*, E05S02. https://doi.org/10.1029/2005JE002605

Michael, G. G. (2013). Planetary surface dating from crater size–frequency distribution measurements: Multiple resurfacing episodes and differential isochron fitting. *Icarus*, *226*, 885–890. https://doi.org/10.1016/j.icarus.2013.07.004

Michael, G. G., Platz, T., Kneissl, T., & Schmedemann, N. (2012). Planetary surface dating from Crater size–frequency distribution measurements: Spatial randomness and clustering. *Icarus*, *218*, 169–177. https://doi.org/10.1016/j.icarus.2011.11.033

Neumann, G., Zuber, M., & Smith, D. E. (2003). MOLA mission experiment gridded data record. [Data set]. NASA Planetary Data System. https://doi.org/10.17189/1519460

Ojha, L., & Lewis, K. (2018). The density of the Medusae Fossae Formation: Implications for its composition, origin, and importance in Martian history. *Journal of Geophysical Research: Planets*, *123*(6), 1368–1379. https://doi.org/10.1029/2018JE005565

Ori, G. G., Marinangeli, L., & Baliva, A. (2000). *Terraces and Gilbert-type Deltas in Crater Lakes in Ismenius Lacus and Memnonia* (MARS), (Vol. 105, pp. 629–641). https://doi.org/10.1029/1999je001219

Parker, T. J., Gorsline, D. S., Saunders, R. S., Pieri, D. C., & Schneeberger, D. M. (1993). Coastal geomorphology of the Martian northern plains. *Journal of Geophysical Research*, *98*(E6), 11. https://doi.org/10.1029/93JE00618

Rice, M. S., Bell, J. F., III, Gupta, S., Warner, N. H., & Anderson, R. B. (2013). A detailed geologic characterization of Eberswalde crater, Mars. Mars. *The International Journal of Mars Science and Exploration*, *8*, 15–57. https://doi.org/10.1555/mars.2013.0002

Rivera-Hernández, F., & Palucis, M. C. (2019). Do deltas along the crustal dichotomy boundary of Mars in the Gale crater region record a northern ocean? *Geophysical Research Letters*, *46*, 8689–8699. https://doi.org/10.1029/2019GL083046

Scott, D. H., & Tanaka, K. L. (1986), *Geologic map of the western equatorial region of Mars*, USGS Miscellaneous Investigations Series Map I-1802-A, scale1:500,000.

Sholes, S. F., Dickeson, Z. I., Montgomery, D. R., & Catling, D. C. (2021). Where are Mars' hypothesized ocean shorelines? Large lateral and topographic offsets between different versions of paleoshoreline maps. *Journal of Geophysical Research: Planets*, *126*, e2020JE006486. https://doi.org/10.1029/2020JE006486

Singh, A., Thomsen, K. J., Sinha, R., Buylaert, J.-P., Carter, A., Mark, D. F., et al. (2017). Counter-intuitive influence of Himalayan river morphodynamics on Indus Civilisation urban settlements. *Nature Communications*, *8*(1), 1617. https://doi.org/10.1038/s41467-017-01643-9

Stucky de Quay, G., Goudge, T. A., & Fassett, C. I. (2020). Precipitation and aridity constraints from paleolakes on early Mars. *Geology*, *48*, 1189–1193. https://doi.org/10.1130/G47886.1

Tanaka, K. L., Skinner, J. A., Dohm, J. M., Irwin, R. P., Kolb, E. J., Fortezzo, C. M., et al. (2014). *Geologic Map of Mars* (Vol. 3292). USGS Scientific Investigations Series Map. https://doi.org/10.3133/sim3292.scale 1:20,000,000.

Thomas, N., Cremonese, G., Ziethe, R., Gerber, M., Brändli, M., Bruno, G., et al. (2017). The Colour and stereo surface imaging system (CaSSIS) for the ExoMars trace gas orbiter. *Space Science Reviews*, *212*(3–4), 1897–1944. https://doi.org/10.1007/s11214-017-0421-1

Ventra, D., & Clarke, L. E. (2018). *Geology and Geomorphology of Alluvial and Fluvial Fans: Current Progress and Research Perspectives* (Vol. 440, pp. 1–21). Geological Society Special Publication. https://doi.org/10.1144/SP440.16

Warner, N. H., Gupta, S., Calef, F., Grindrod, P., Boll, N., & Goddard, K. (2015). Minimum effective area for high resolution crater counting of Martian terrains. *Icarus*, *245*, 198–240.

Williams, R. M. E., Irwin, R. P., & Zimbelman, J. R. (2009). Evaluation of paleohydrologic models for terrestrial inverted channels: Implications for application to martian sinuous ridges. *Geomorphology*, *107*, 300–315. https://doi.org/10.1016/j.geomorph.2008.12.015

Williams, R. M. E., & Weitz, C. M. (2014). Reconstructing the aqueous history within the southwestern Melas basin, Mars: Clues from stratigraphic and morphometric analyses of fans. *Icarus*, *242*, 19–37. https://doi.org/10.1016/j.icarus.2014.06.030

Wilson, S. A., Morgan, A. M., Howard, A. D., & Grant, J. A. (2021). The global distribution of craters with alluvial fans and deltas on Mars. *Geophysical Research Letters*. https://doi.org/10.1029/2020gl091653.in press.

Zimbelman, J. R., & Griffin, L. J. (2010). HiRISE images of yardangs and sinuous ridges in the lower member of the Medusae Fossae Formation, Mars. *Icarus*, *205*, 198–210. https://doi.org/10.1016/j.icarus.2009.04.003

Zuber, M. T., Smith, D. E., Solomon, S. C., Muhleman, D. O., Head, J. W., Garvin, J. B., et al. (1992). The Mars Observer laser altimeter investigation. *Journal of Geophysical Research*, *97*, 7781–7797. https://doi.org/10.1029/92JE00341